# *PROPERTIES OF A SAMPLE OF THE MOST COMPACT RADIO GALAXIES*

*M.Sci. Emily Kosmaczewski*

*Doctoral Candidate*

*Department Of High Energy Astrophysics*

*Astronomical Observatory Of Jagiellonian University*

*Emily@oa.uj.edu.pl*

*L. Stawarz (Astronomical Observatory Of UJ)*

*A. Siemiginowska (Harvard-Smithsonian Center For Astrophysics)*

*C.C. Cheung (Naval Research Laboratory)*

*L. Ostorero (Universita Degli Studi Di Torino And Instituto Nazionale Di Fisica Nucleare)*

*M. Sobolewska (Harvard-Smithsonian Center For Asrophysics)*

*D. Koziel-wierzbowska (Astronomical Observatory Of UJ)*

*A. Wojtowicz (Astronomical Observatory Of UJ)*

*V. Marchenko (Astronomical Observatory Of UJ)*

1. Selecting our Sample
2. Mid-infrared data
3. WISE Data/Analysis
4. Optical Classifications
5. IR/Xray Correlation
6. Gamma Detection (Fermi-Lat)
7. Conclusions & Next Steps

# *Overview*

# *OUR SAMPLE*

# Our Sample

- We consider only radio galaxies for which:
  - Redshifts are measured
  - Characterized by compact radio structures with linear sizes LS<1 kpc
  - Classified morphologically as Compact Symmetric Objects (CSOs) and/or spectrally as GHz-peaked spectrum (GPS) sources
  - Has available (good) X-ray data
- This amounts to a total of 29 targets
  - Including 27 that have been detected in X-rays by either XMM-Newton or Chandra
  - 1 source with the X-ray flux measured by ASCA, 1146+596
  - 1 source having a Chandra upper limit for its 0.5-2.0keV flux, 0116+319

| Name | $z$ | $d_L$ [Mpc] | LS [pc] | class |
|---|---|---|---|---|
| (1) | (2) | (3) | (4) | (5) |
| 0019–000 | 0.305 | 1521 | 220 | GPS |
| 0026+346 | 0.517 | 2852 | 190 | GPS |
| 0035+227 | 0.096 | 418 | 21.8 | CSO |
| 0108+388 | 0.669 | 3907 | 22.7 | CSO |
| 0116+319 | 0.059 | 255 | 70.1 | CSO |
| 0402+379 | 0.055 | 234 | 7.3 | CSO |
| 0428+205 | 0.219 | 1044 | 653 | GPS |
| 0500+019 | 0.585 | 3319 | 55 | GPS |
| 0710+439 | 0.518 | 2868 | 87.7 | CSO |
| 0941–080 | 0.228 | 1100 | 148 | GPS |
| 1031+567 | 0.460 | 2480 | 109 | CSO |
| 1117+146 | 0.362 | 1874 | 306 | GPS |
| 1146+596 | 0.011 | 47 | 933$^{\diamond}$ | CSO$^{\bullet}$ |
| 1245+676 | 0.107 | 478 | 9.6 | CSO |
| 1323+321 | 0.368 | 1908 | 247 | GPS |
| 1345+125 | 0.122 | 551 | 166 | CSO |
| 1358+624 | 0.431 | 2298 | 218 | GPS |
| 1404+286 | 0.077 | 336 | 10.0 | CSO |
| 1511+0518 | 0.084 | 370 | 7.3 | CSO |
| 1607+268 | 0.473 | 2569 | 240 | CSO |
| 1718–649 | 0.014 | 60.4 | 2.0 | CSO |
| 1843+356 | 0.763 | 4612 | 22.3 | CSO |
| 1934–638 | 0.183 | 845 | 85.1 | CSO |
| 1943+546 | 0.263 | 1285 | 107.1 | CSO |
| 1946+708 | 0.101 | 444 | 39.4 | CSO |
| 2008–068 | 0.547 | 3056 | 218 | CSO |
| 2021+614 | 0.227 | 1086 | 16.1 | CSO |
| 2128+048 | 0.990 | 6364 | 218 | GPS |
| 2352+495 | 0.238 | 1143 | 117.3 | CSO |

# *MID-INFRARED DATA*

- *Limited studies on Compact Radio Galaxies in the Mid/Far- Infrared namely:*
  - Heckman et a. (1994) utilizing IRAS
  - Fanti et al. (2000) utilizing ISO
  - Willett et al. (2010) utilizing Spitzer
- There is a vital need for an update on the MIR/FIR view on young radio sources indeed, especially utilizing the recent and extensive WISE archive which has better resolution than previous instruments.

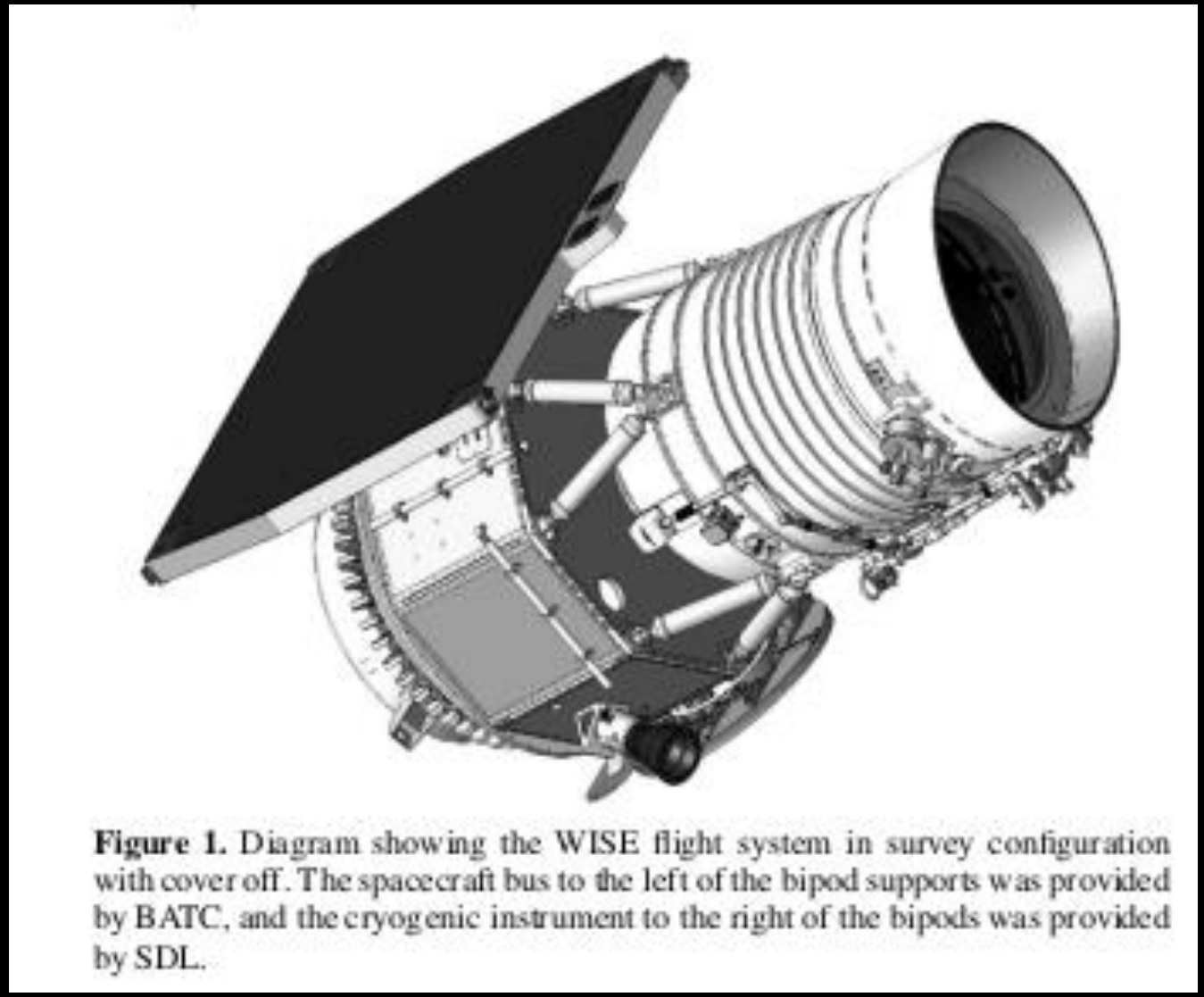

**Figure 1.** Diagram showing the WISE flight system in survey configuration with cover off. The spacecraft bus to the left of the bipod supports was provided by BATC, and the cryogenic instrument to the right of the bipods was provided by SDL.

# *WISE ALL Sky Survey*

- Wide-field Infrared Survey Explorer
- Mapped the whole sky -- 2010
- 40 cm telescope with 4 million pixels
- 5sig point source sensitivites
- 4 bands

  W1 – 3.4 microns

  W2 – 4.6 microns

  W3 – 12 microns

  W4 – 22 microns

Wright et al. 2010

# *WISE Contamination*

- Angular Resolution of WISE
  - W1, W2, W3 bands ~ 6″
- Any bright infrared sources within 6″ will contaminate the wise color diagnostics
- We performed a visual and literature search for any objects within 6″ of our sources
- Two known interacting binary systems, 0941-080 and 1934-638 (see de Vries, et al. (1998) and Jauncey, et al. (1986) respectively)
- Potential contamination found for:
  - *1345+125*
    - *Binary system*
  - *0116+319*
    - *Potential galactic merger*
  - *0941-080*
    - *Interacting binary source*
  - *1934-638*
    - *Two compact companions*

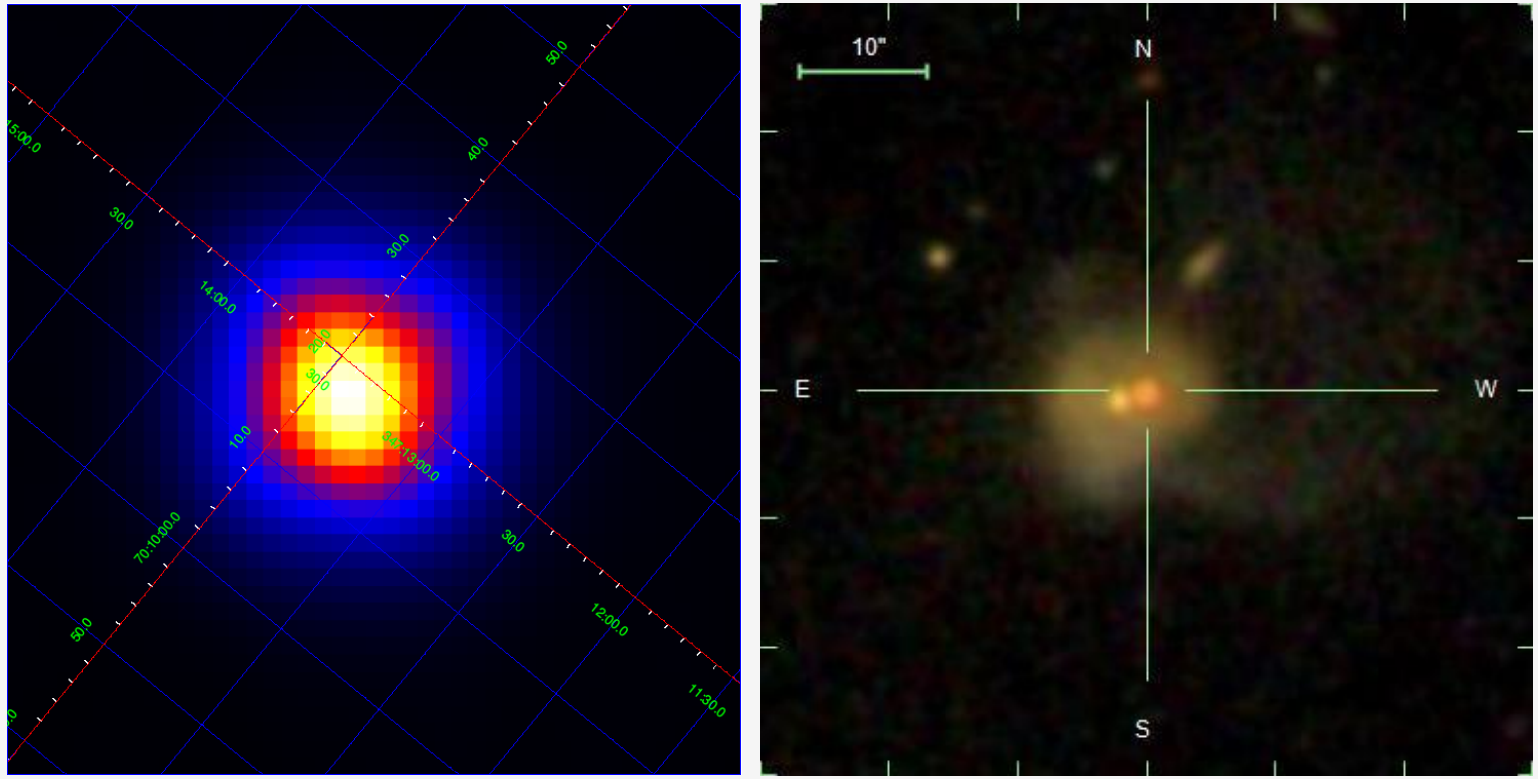


WISE 12 micron images with overlaid ecliptic coordinate grid (left), along with the SDSS gri color composite image (right) for 1345 +125. Images are a square 60".

# *Wise Color Classification*

- Established by Wright et al. 2010
- Colors from magnitude differences in IR bands
- Different objects occupy differing regions correlating to the dust in the system
- Stars/Ellipticals having the lowest and our Obscured AGN having the highest
- Significant overlap prevents this from being a comprehensive classification
- Suggestive of the amount of dust in the system, not necessarily the galactic classification

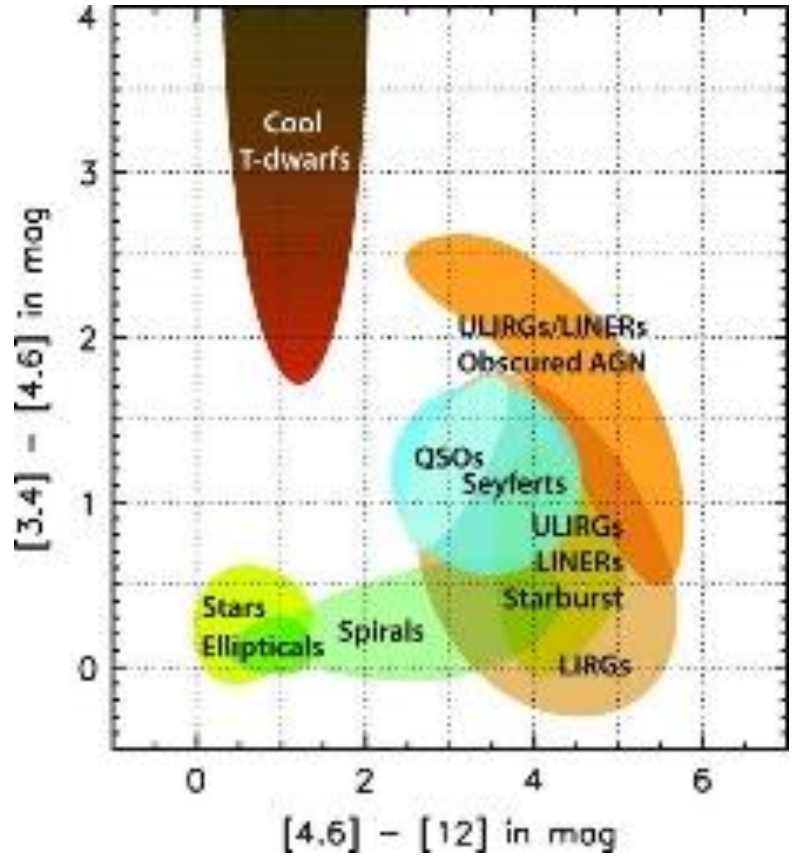


Wright et al. 2010

# *WISE Color-Color Plot*

**Figure:**

- ``Galaxy'' (G) -- green triangle,
- ``Starburst'' (SB) -- purple side-pointing triangle,
- ``Quasar/Seyfert'' (Q/Sy) -- black star,
- ``Uncertain'' (Un) -- black circle
- Black square: may have significant contamination from nearby objects
- Red circle: objects confirmed as Compton-thick based on X-ray spectroscopy

- The horizontal solid line delineates the Stern et al. (2012) cut: the MIR emission of sources located above the line is dominated by an AGN component.
- The dotted, dashed lines show the Mateos et al. (2012) cut: the MIR emission of sources located within wedge is dominated by an AGN component.

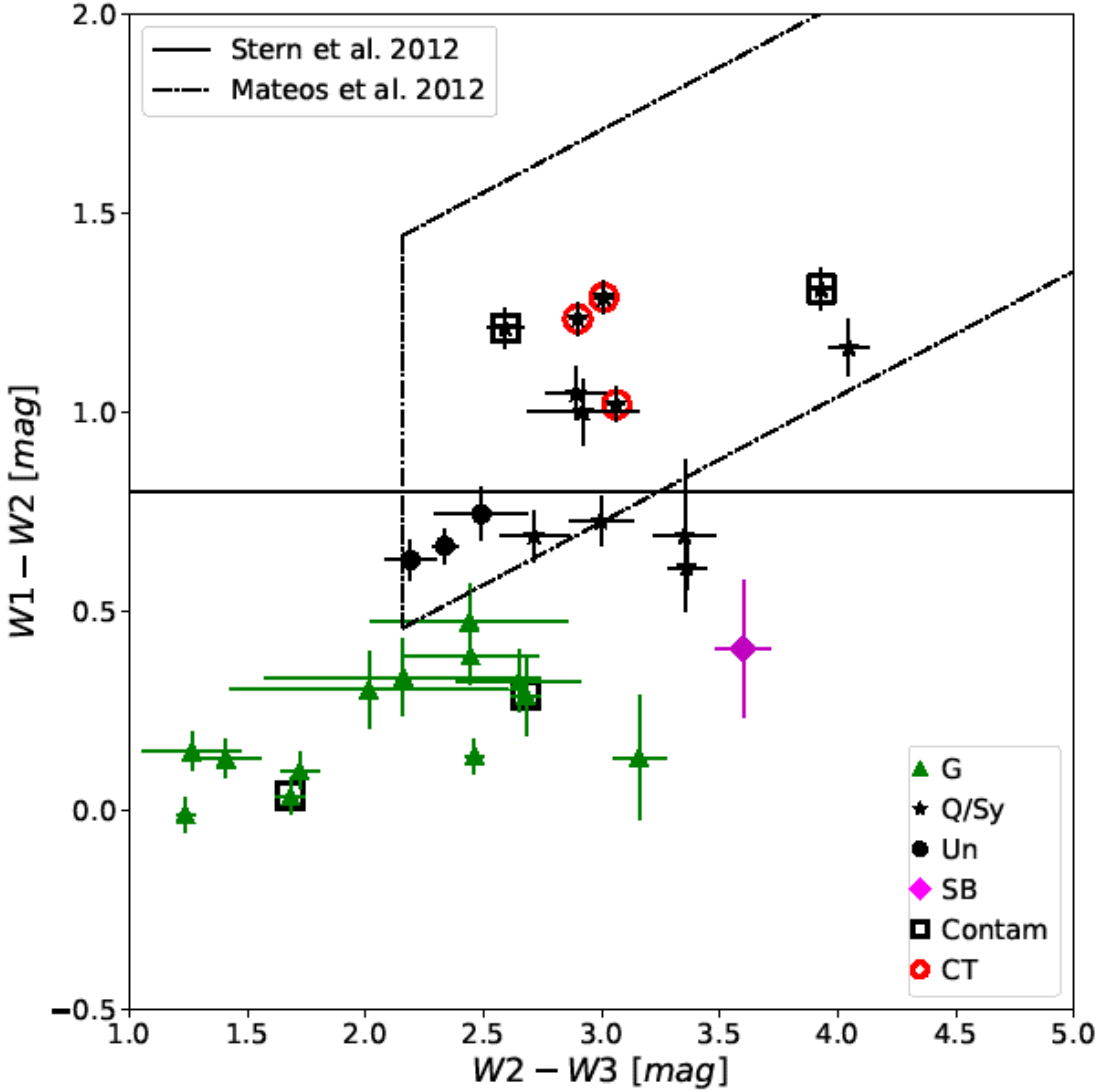

# *WISE Classification*

- Variety of colors across the sample
- MIR continua are contributed to by the circumnuclear dust and ISM of the host galaxies
- Suggests the sources have varying levels of star formation
- Due to overlap of regions there is a level of bias introduced in the identifications
- Note that these colors are based on the entire galaxy not just the nuclear regions

| Name | $z$ | $d_L$ [Mpc] | LS [pc] | class | W1–W2 [mag] | W2–W3 [mag] | *WISE* color |
|---|---|---|---|---|---|---|---|
| (1) | (2) | (3) | (4) | (5) | (6) | (7) | (8) |
| 0019–000 | 0.305 | 1521 | 220 | GPS | 0.472 | 2.441 | G |
| 0026+346 | 0.517 | 2852 | 190 | GPS | 0.743 | 2.491 | Un |
| 0035+227 | 0.096 | 418 | 21.8 | CSO | 0.148 | 1.265 | G |
| 0108+388 | 0.669 | 3907 | 22.7 | CSO | 0.132 | 3.159 | G |
| 0116+319 | 0.059 | 255 | 70.1 | CSO | 0.035 | 1.682 | S* |
| 0402+379 | 0.055 | 234 | 7.3 | CSO | 0.099 | 1.721 | G |
| 0428+205 | 0.219 | 1044 | 653 | GPS | 0.323 | 2.648 | G |
| 0500+019 | 0.585 | 3319 | 55 | GPS | 1.047 | 2.892 | Q |
| 0710+439 | 0.518 | 2868 | 87.7 | CSO | 0.726 | 2.997 | Sy |
| 0941–080 | 0.228 | 1100 | 148 | GPS | 0.388 | 2.444 | G* |
| 1031+567 | 0.460 | 2480 | 109 | CSO | 0.999 | 2.922 | Q |
| 1117+146 | 0.362 | 1874 | 306 | GPS | 0.406 | 3.599 | SB |
| 1146+596 | 0.011 | 47 | 933° | CSO• | –0.011 | 1.237 | G |
| 1245+676 | 0.107 | 478 | 9.6 | CSO | 0.130 | 1.409 | G |
| 1323+321 | 0.368 | 1908 | 247 | GPS | 0.303 | 2.014 | G |
| 1345+125 | 0.122 | 551 | 166 | CSO | 1.308 | 3.930 | Sy* |
| 1358+624 | 0.431 | 2298 | 218 | GPS | 1.210 | 2.592 | Q* |
| 1404+286 | 0.077 | 336 | 10.0 | CSO | 1.018 | 3.063 | Q |
| 1511+0518 | 0.084 | 370 | 7.3 | CSO | 1.233 | 2.899 | Q |
| 1607+268 | 0.473 | 2569 | 240 | CSO | 0.287 | 2.679 | S* |
| 1718–649 | 0.014 | 60.4 | 2.0 | CSO | 0.136 | 2.462 | G |
| 1843+356 | 0.763 | 4612 | 22.3 | CSO | 1.160 | 4.047 | Sy |
| 1934–638 | 0.183 | 845 | 85.1 | CSO | 0.609 | 3.360 | Sy* |
| 1943+546 | 0.263 | 1285 | 107.1 | CSO | 0.628 | 2.191 | Un |
| 1946+708 | 0.101 | 444 | 39.4 | CSO | 0.663 | 2.336 | Un |
| 2008–068 | 0.547 | 3056 | 218 | CSO | 0.334 | 2.159 | G |
| 2021+614 | 0.227 | 1086 | 16.1 | CSO | 1.287 | 3.009 | Q |
| 2128+048 | 0.990 | 6364 | 218 | GPS | 0.688 | 3.352 | Sy |
| 2352+495 | 0.238 | 1143 | 117.3 | CSO | 0.688 | 2.714 | Sy |

# *Comparison of Samples*

- **Asmus et al. (2014)**
  - **Sample of local (z<0.4) Seyferts & LINERs**
  - **Selected based on X-ray and MIR properties**
  - **Sample of both radio-loud and radio-quiet sources**
- AGN sample of local Seyferts and LINERs with our sample of 29 GPS/CSO sources.
- Quality cuts for Asmus et al. (2014)
  - Remove sources with a <1 SNR for W1, W2, & W3 bands
  - Remove cc_flag sources
    - Sources marked as contaminated by WISE system
  - Results in a sample of 121 sources

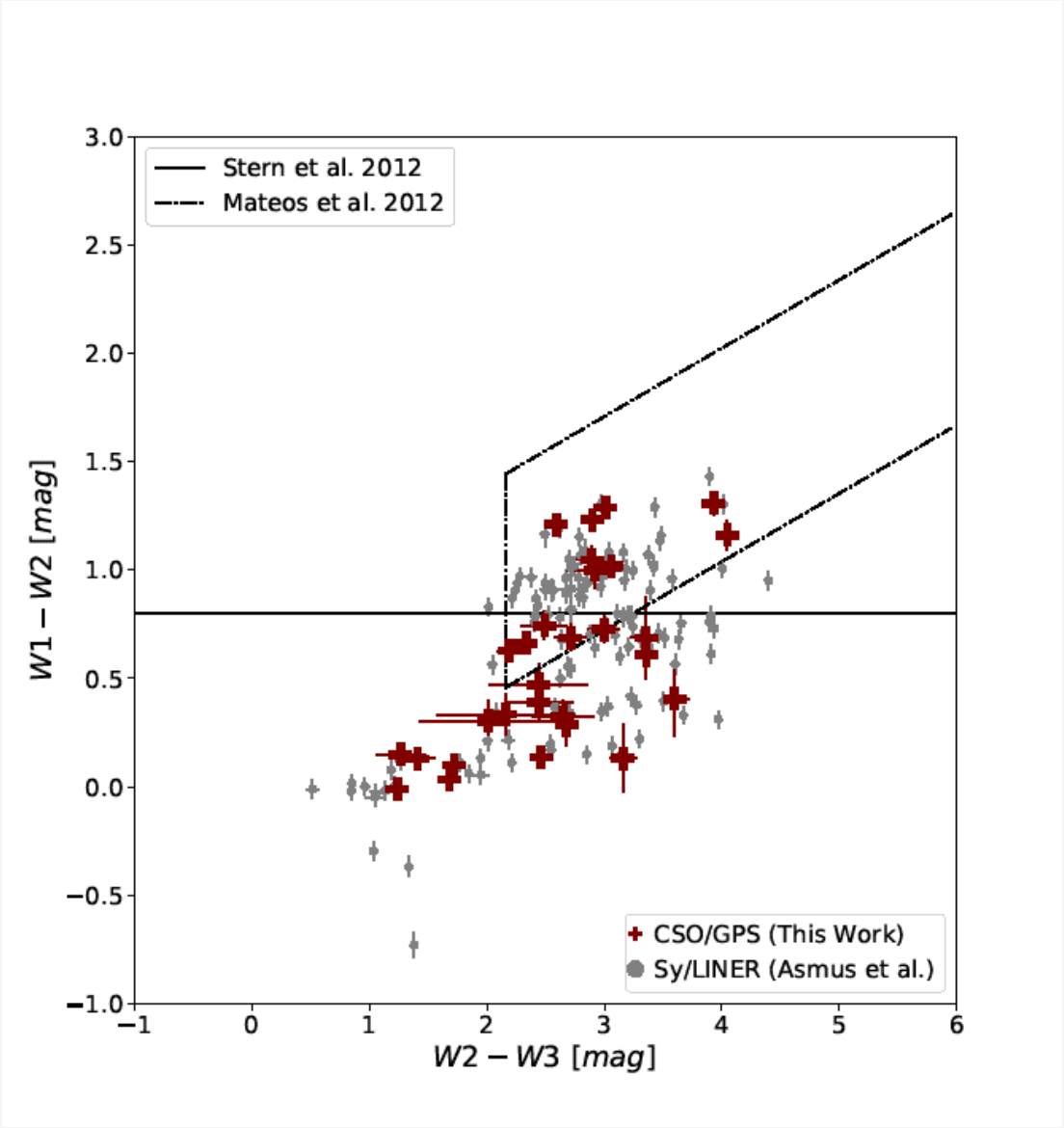

# *KS Test Statistics*

- Two-dimensional Kolmogorov-Smirnov (2D KS) test, that was developed through the efforts to generalize the classical one-dimensional KS test to two (see Peacock et al. 1983) and higher dimensions (see Fasano et al. 1987)
- In particular, we follow the 2D KS algorithm described in Fasano et al. (1987)
  - under the null hypothesis that the two analyzed samples were drawn from the same distribution
  - calculate the two-tailed p-value (i.e., the probability of obtaining a value of the statistic D greater than the observed value, if the null-hypothesis were true).
- Significance level $\alpha = 0.05$
- As a result a p-value of greater than 0.05 will result in the null hypothesis to be accepted
- Alternatively less than 0.05 would be rejected

# *Asmus et al. KS test*

- **Asmus et al. (2014)**
- AGN sample of local Seyferts and LINERs with our sample of 29 GPS/CSO sources.
- *p*-value: 0.0795
- D value: 0.282

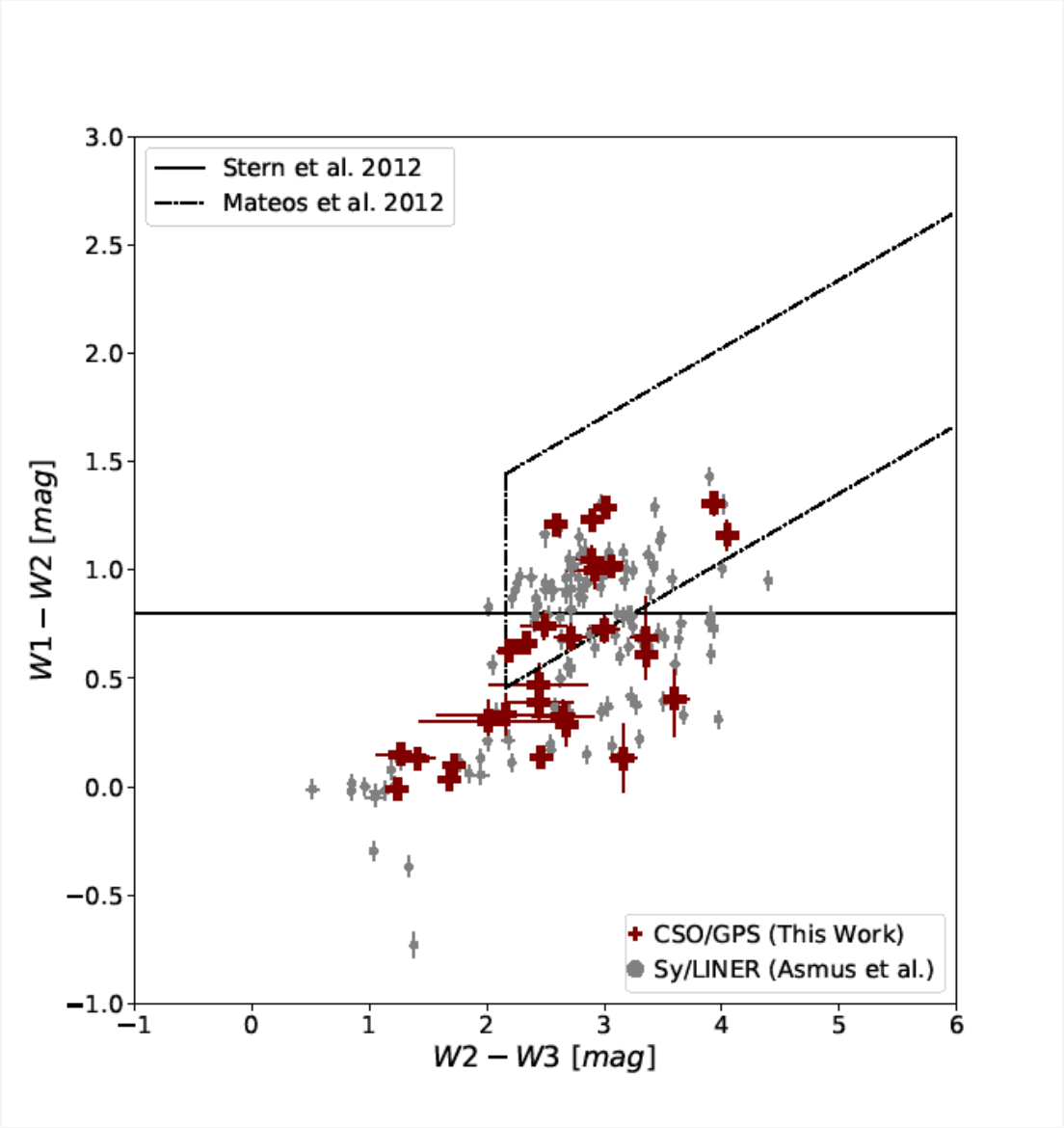

# *Kuzmicz et al. KS test*

- **Kuzmicz et al. (2014)**
  - **Double Double Radio Galaxies**
  - **Two distinct epochs of jet activity**
- Sample of restarted radio galaxies (DDRGs) with our sample of 29 GPS/CSO sources.
- *p*-value: 0.065
- D-value: 0.31

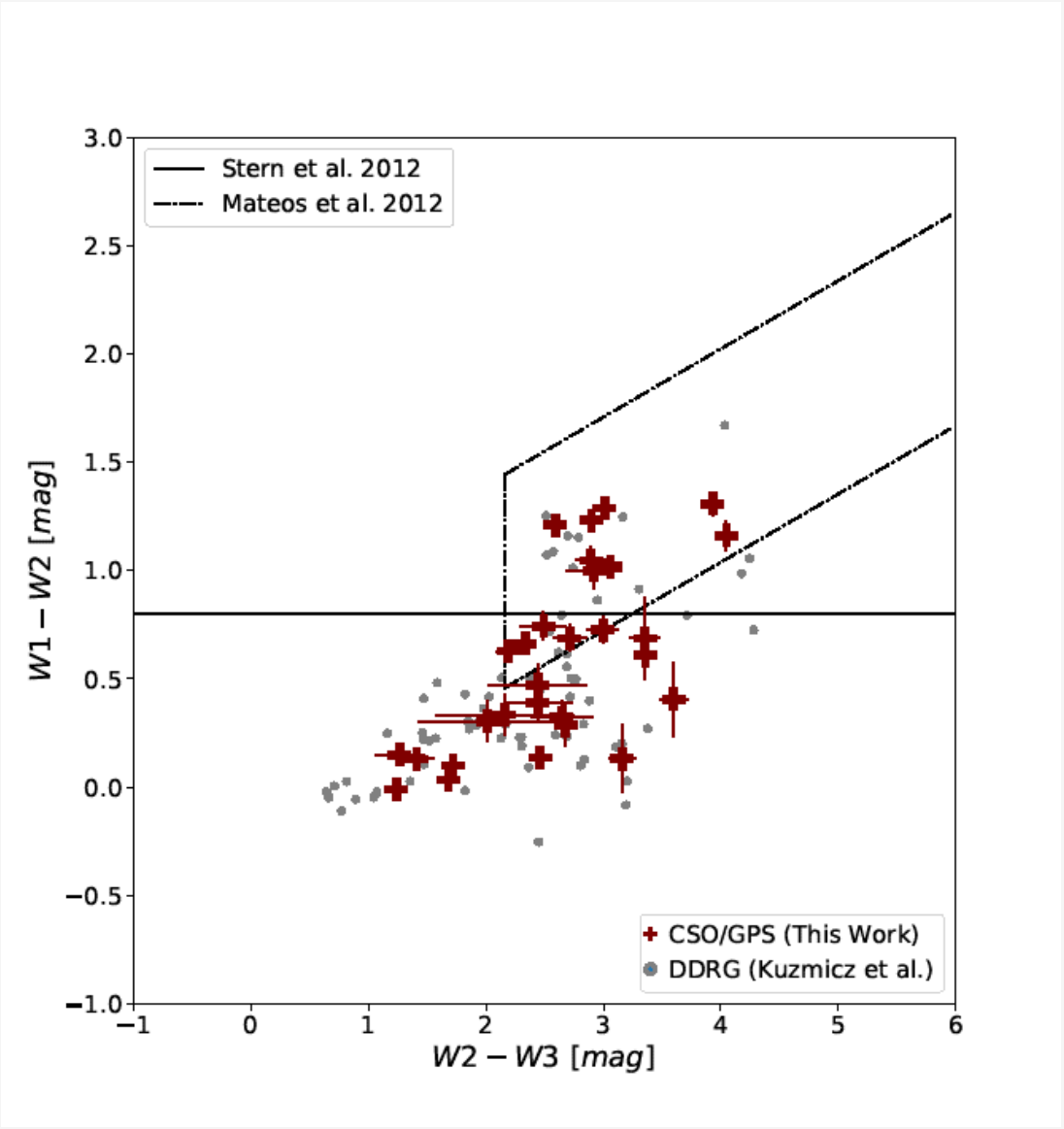

# *Koziel-Wierzbowska, & Stasinska et al. KS test*

- **Koziel-Wierzbowska, & Stasinska et al. (2011)**
  - **Evolved FRII type Radio Galaxies**
  - **Cross identification of 3C-9C radio catalog with optical SDSS DR7**
- Sample of evolved classical doubles (FR II-type radio galaxies) with our sample of 29 GPS/CSO sources.
- *p*-value: 0.95x10^-7
- D-value: 0.60

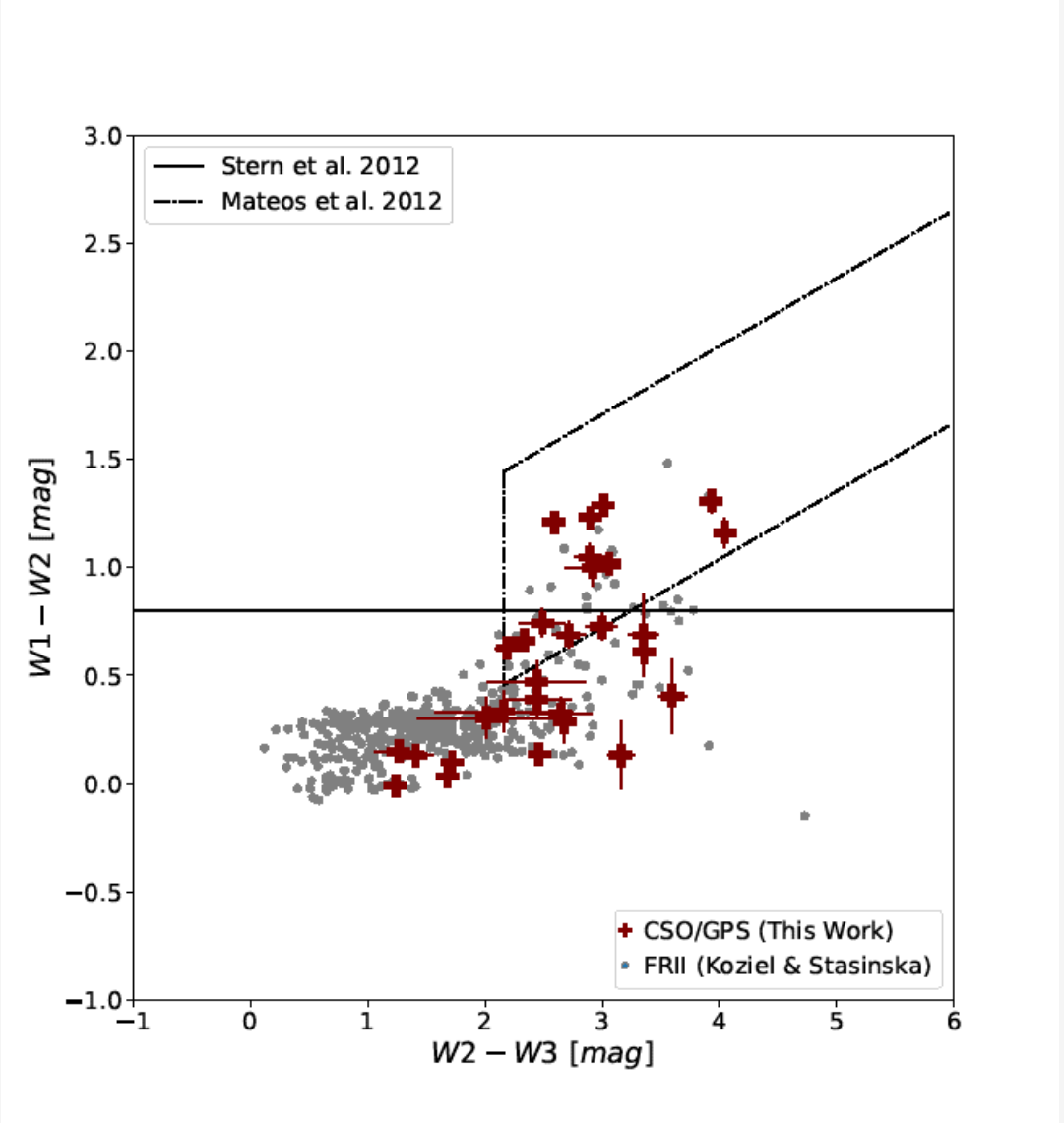

# *Van Velzen et al. KS test*

- **Van Velzen et al. (2015)**
  - **Sample of evolved double-lobed radio galaxies**
  - **Selected based on an algorithm applied to the FIRST survey**
  - **Expected to be predominantly FRII type radio galaxies, but can have significant overlap with other types of objects**
- Sample of double-lobed radio sources with our sample of 29 GPS/CSO sources.
- Same cuts as Asmus sample
- 9,740 sources
- *p*-value: 0.0028
- D-value: 0.37

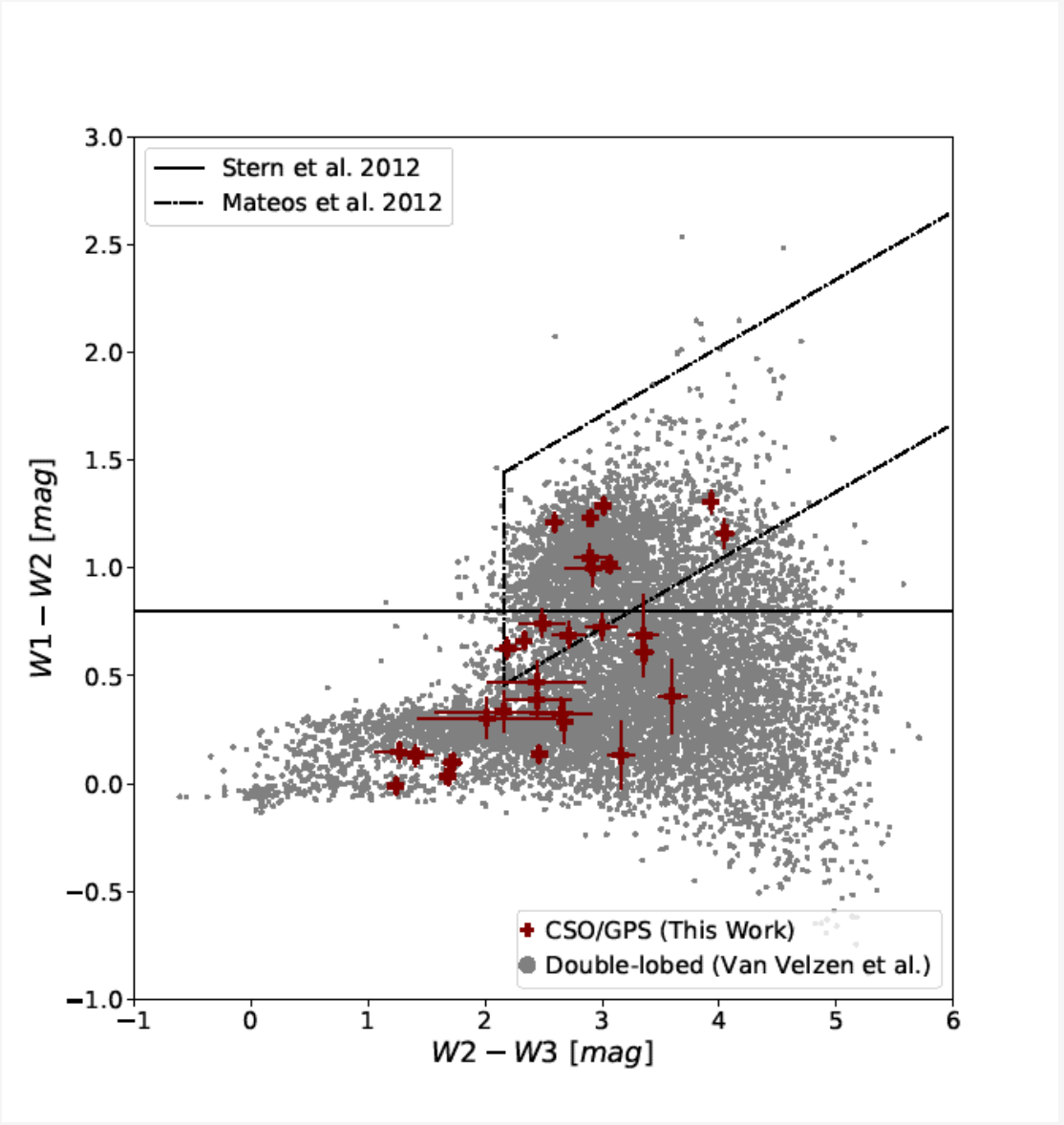

# *Xray Properties of Young Radio Galaxies*

- Young/compact radio galaxies are relatively weak X-ray emitters
  - Small angular sizes make it difficult (or, in most of the cases, simply impossible) to resolve in X-rays
- Systematic X-ray studies of GPS/CSOs with high-angular resolution telescopes reported/summarized in Tengstrand et al. 2009 (XMM-Newton) and Siemiginowska et al. 2016 (Chandra)
- Spectra could be accommodated by either:
  - the disk coronal emission scenario, with modest intrinsic absorption,
  - Or the model in which observed X-ray fluxes are dominated by non-thermal emission of compact radio lobes
- Dedicated deep Chandra/XMM-Newton/Nu-STAR observations of a few/several selected targets, reveal iron fluorescence lines and high absorbing column densities, both consisted with the disk scenario (Sobolewska et al. 2019a,b)

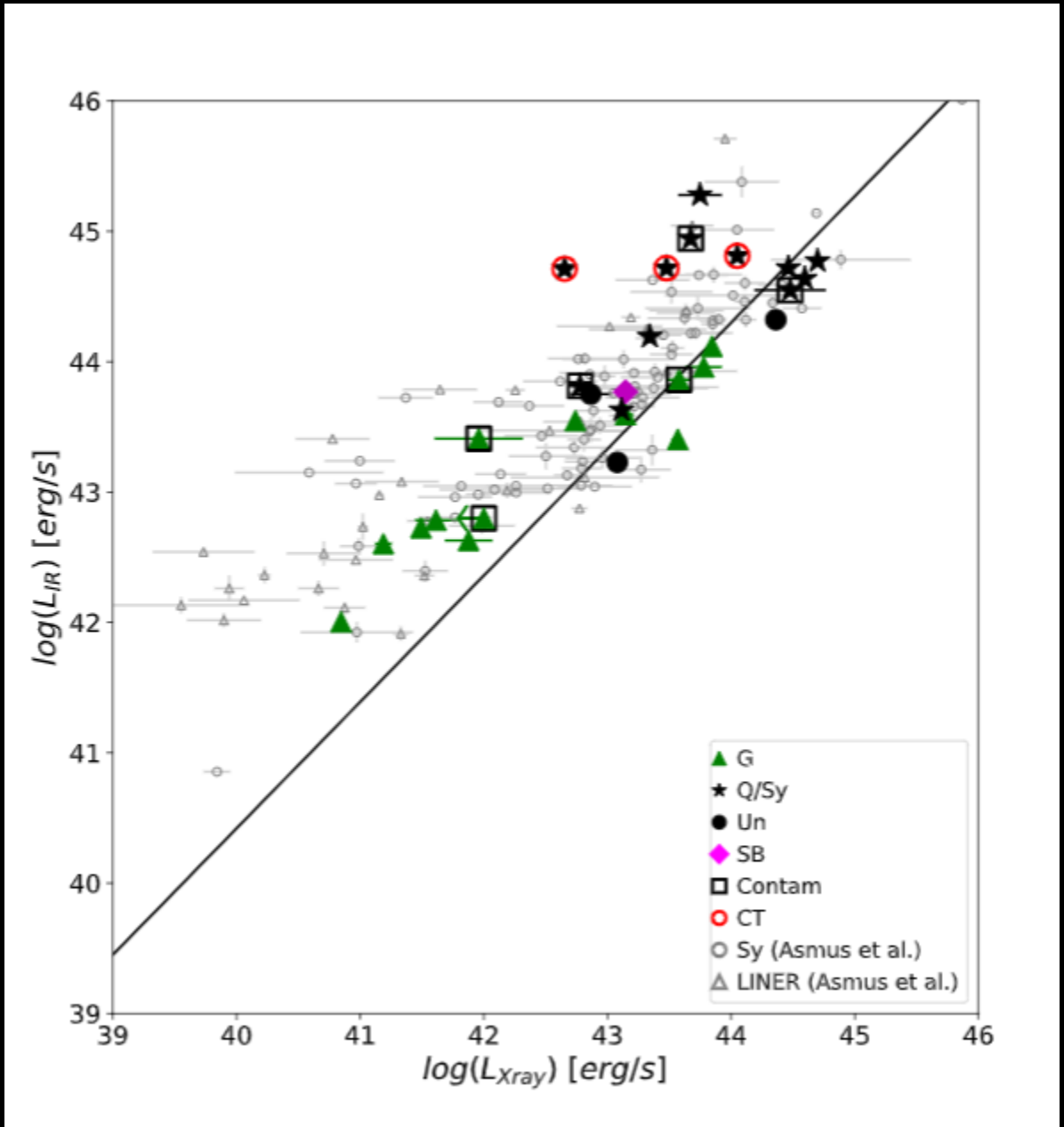


# MIR/XRAY Correlation

- Relation of the WISE 12-micron and the intrinsic (absorption-corrected) 2--10keV luminosities for our compact radio galaxies denoted by large symbols.
- Source 0116+319 has an upper limit X-ray luminosity and is marked with a left pointing arrow, visible on the lower left end of the plot.
- The solid line shows the correlation established for nearby AGN by Asmus et al. (2015) based on the high-angular resolution MIR (ground-based) observations.
- Small grey symbols denote the AGN from the Asmus et al. (2014) sample with IRAS 12-micron luminosities.

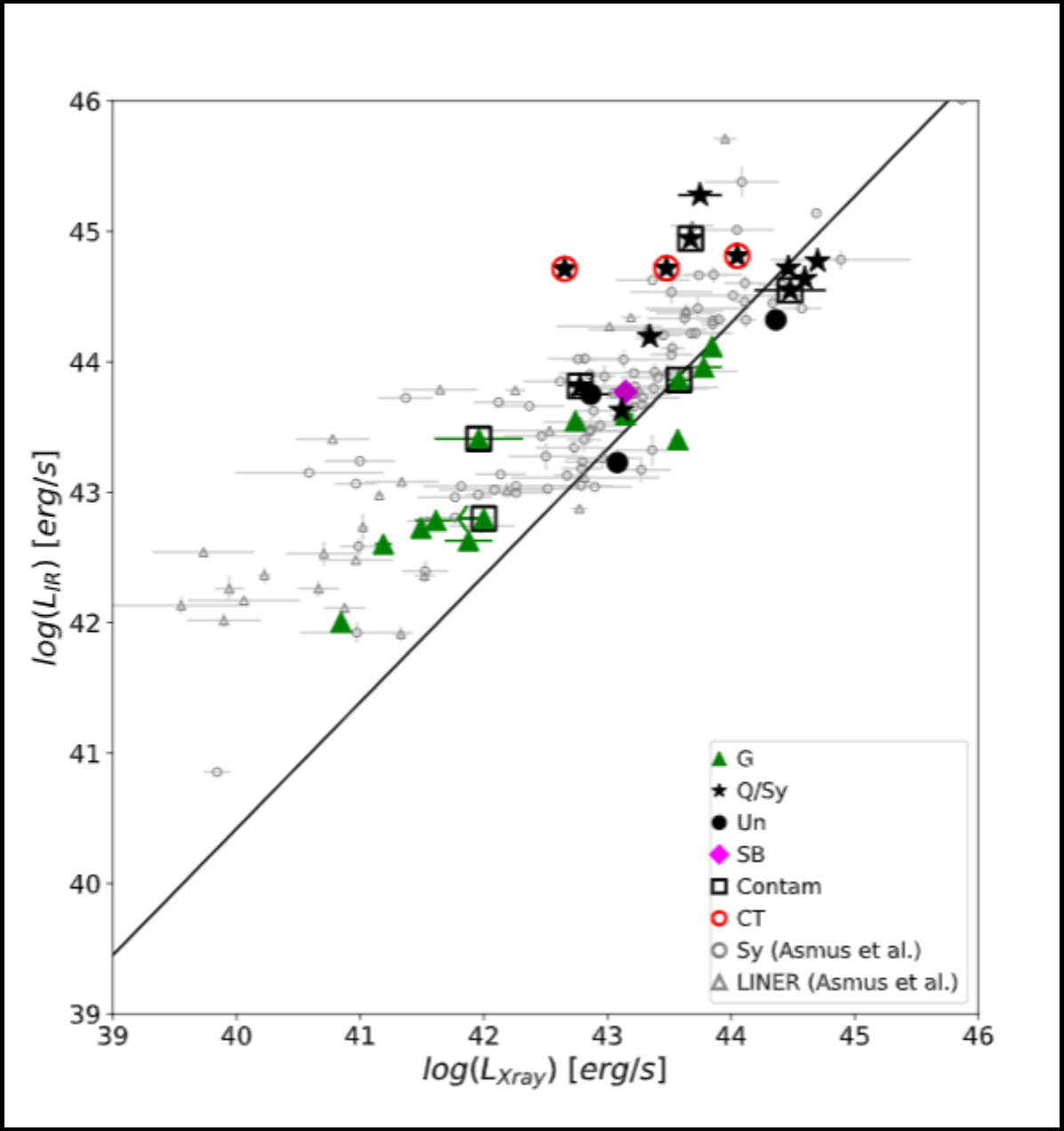


# MIR/XRAY Correlation

- Asmus et al. 2015
- Tight correlation between the 'nuclear' MIR luminosities and the 2-10keV luminosities
- WISE band 3 (12micron)
- Intrinsic (absorption corrected) 2-10keV luminosities
- Seyfert/LINERS plotted in grey from the Asmus et al. 2014 sample.

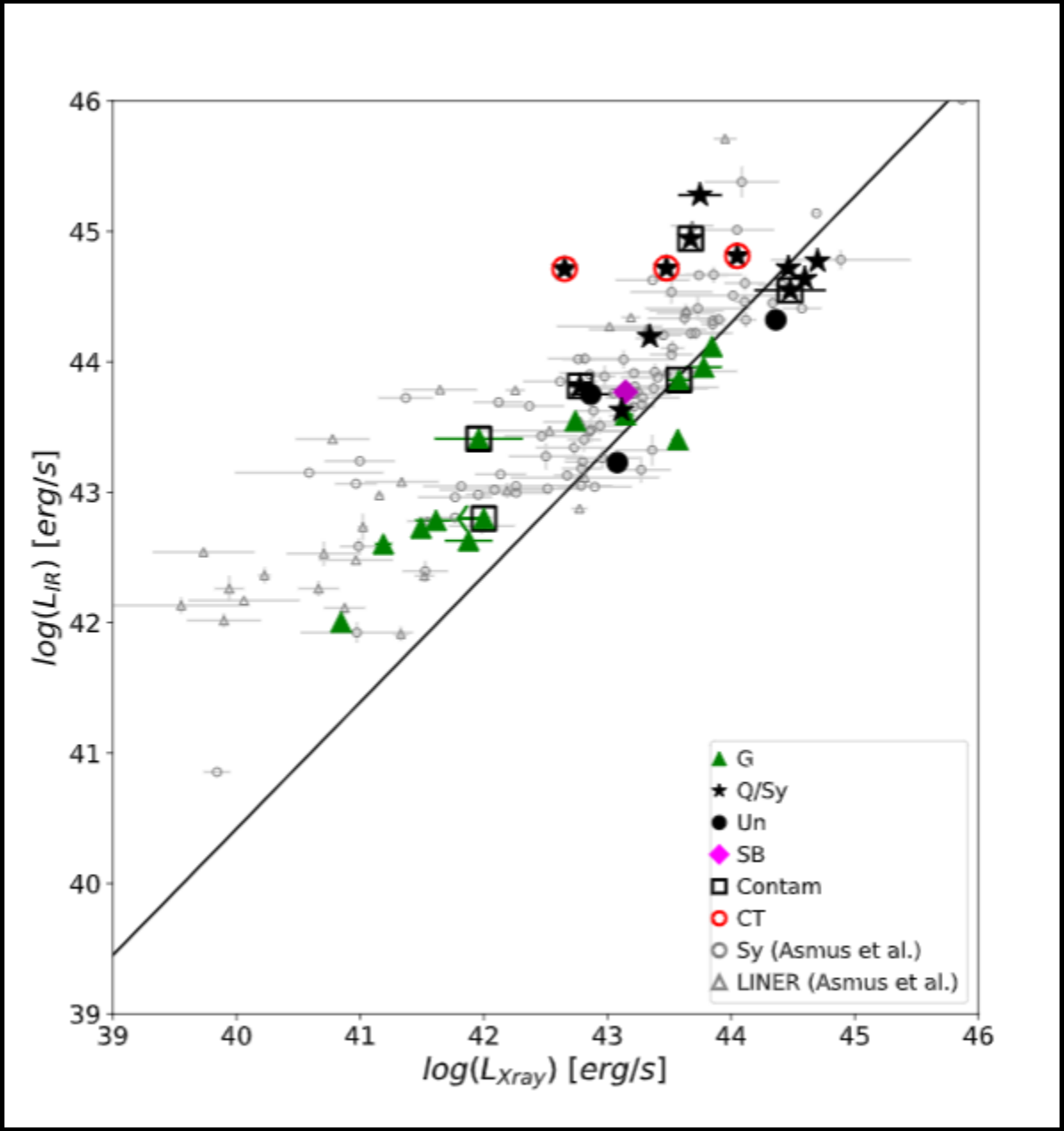


# *MIR / XRAY Correlation*

- The distribution of young radio galaxies in the diagram, at the first glance, resembles the distribution of the comparison local AGN sample.
- The emerging approximate linear scaling between the MIR and X-ray luminosities, along the correlation established by Asmus et al. 2015, could be therefore considered as an indication for the nuclear (disk corona) origin of the observed X-ray fluxes also in the GPS/CSOs sample.

# *Redshift inspection*

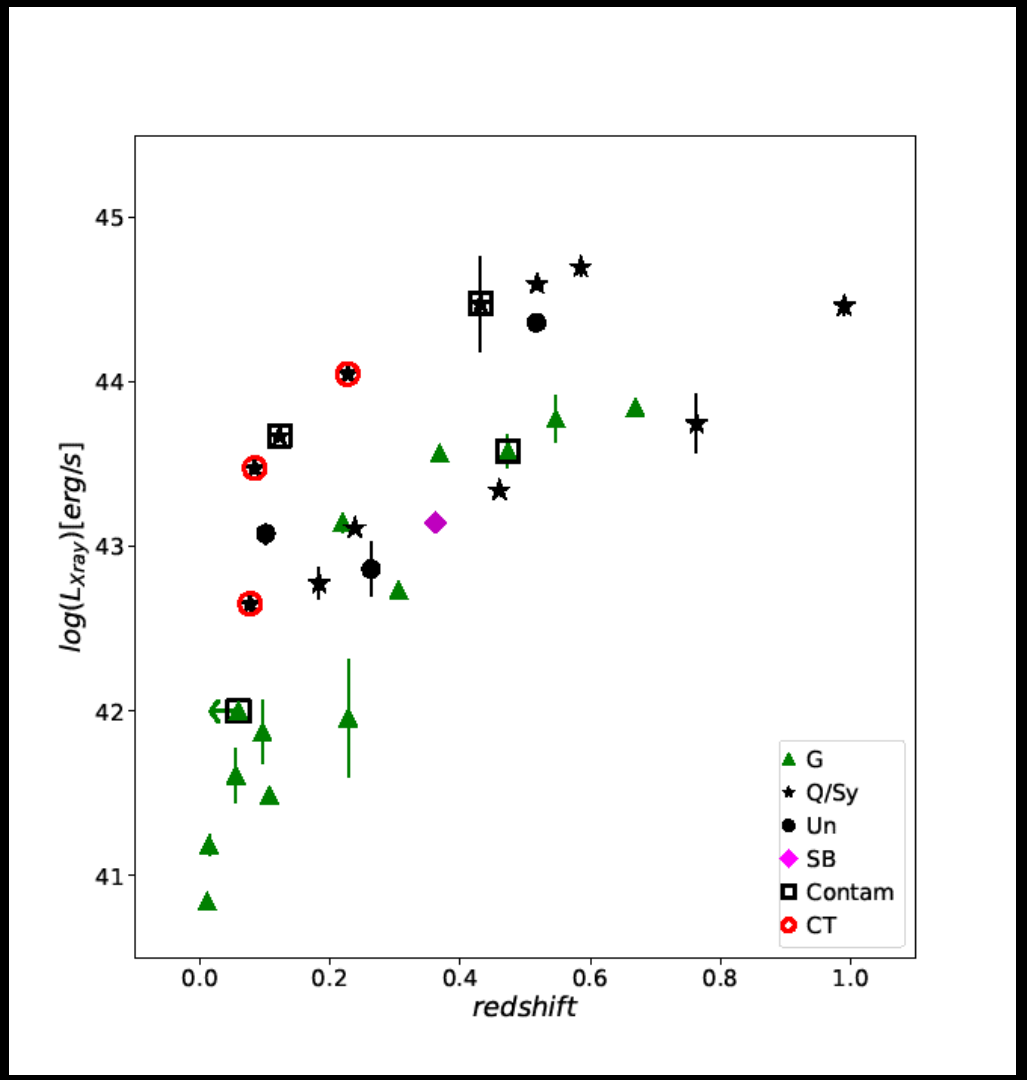


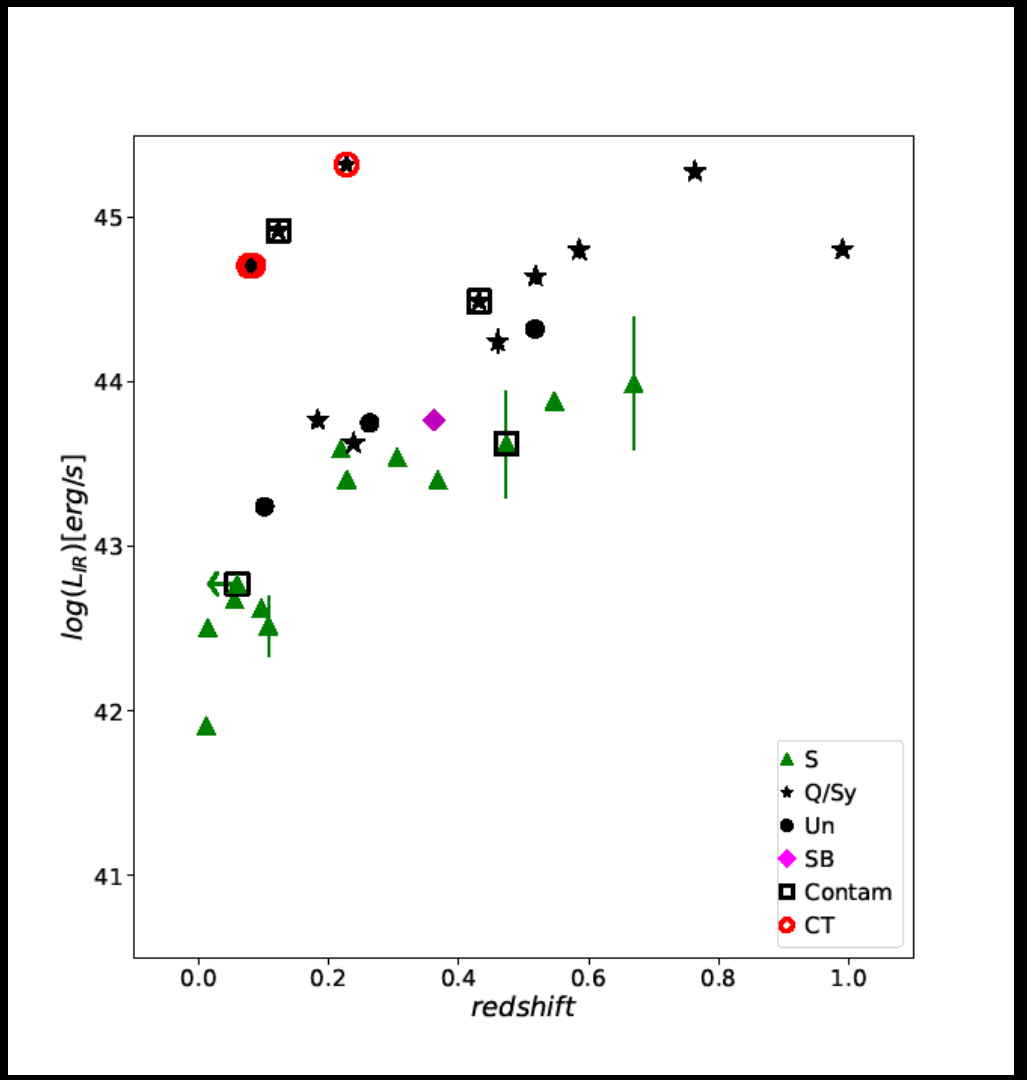

# *Gamma Detection 1718-649*

- Linear size= ~2 pc
- Kinematic age= ~100yr
- Luminosity Distance= 60 Mpc
- The fist bona-fide CSO detected in the high-energy gamma-ray range (Migliori et al. 2016)

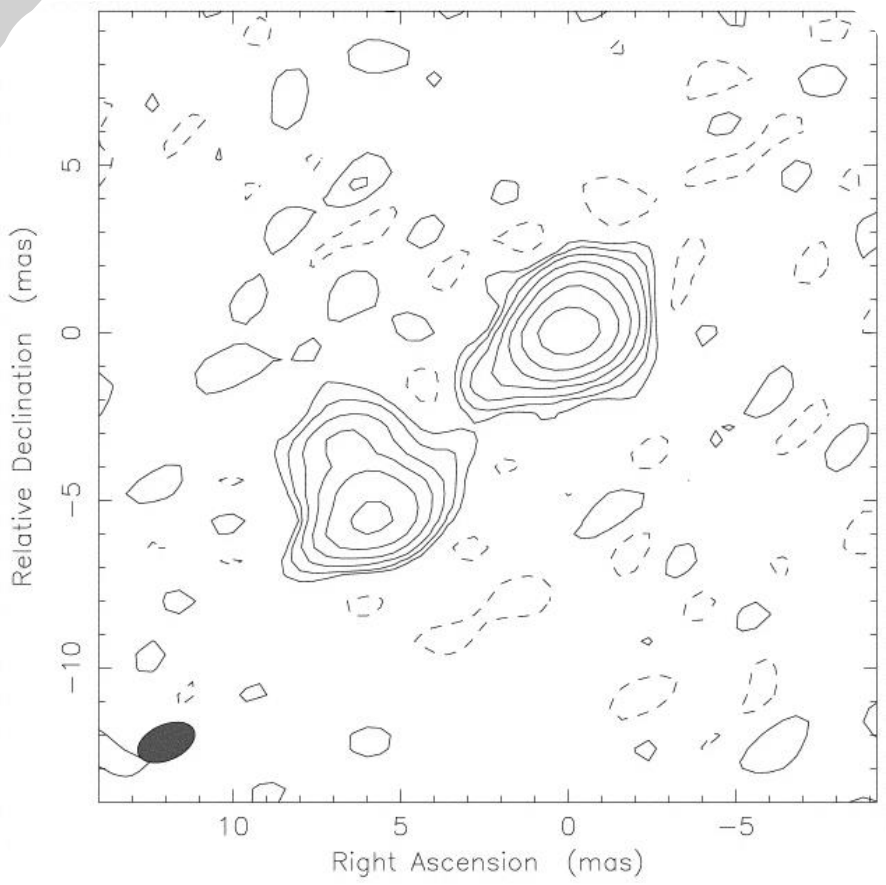


VLBI image of PKS 1718-649 at 22 GHz.
**S. J. TINGAY & M. DE KOOL (2003)**

# *Gamma Detection 1146+59*

- Linear size = 933 pc (Taylor et al ‘98, Perlman et al, 2001)
- Luminosity Distance = 47 Mpc
- Associated with the gamma-ray source 4FGL J1149.0+5924 in the Fermi LAT 8-Year Point Source Catalog
- Note: 1146+596 is characterized by multiple radio outbursts
  - The most compact radio component:
    - Kinematic age: ~60 yr
    - Linear size: ~3.5 pc (Principe et al. 2020)

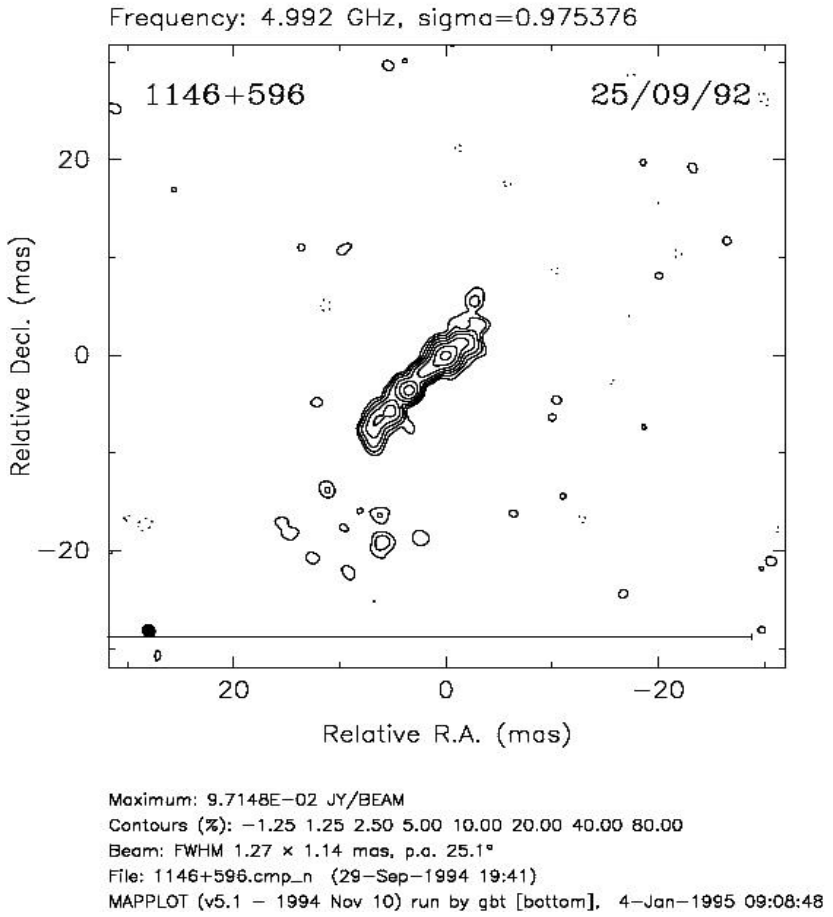


Image courtesy of NED

# *Fermi-LAT*

- 1718--649 and 1146+596 are the two lowest-luminosity sources in our sample, which are rather unique objects for several reasons.
- The question follows if the observed gamma-ray emission in both sources is :
  - related to the jet activity and the compact radio lobes
  - Or is it due to the star formation activity within the hosts, analogous to the LAT-detected, star-forming and starburst galaxies
- Integrated infrared flux can estimate the respective star formation rate

$$\frac{SFR}{M_{sun} yr^{-1}} = \epsilon 1.7 * \frac{L_{8-1000\mu m}}{10^{10} L_{sun}}$$

- Initial mass function factor $\epsilon = 0.79$ (Ackermann et al. 2012)
- From the integrated infrared luminosities we can estimate the gamma-ray luminosity from the star formation activity

$$\log\left(\frac{L_{0.1-100GeV}}{10^{39} erg\ s^{-1}}\right) = 1.17 \log\left(\frac{L_{8-1000\mu m}}{10^{10} L_{sun}}\right) + 0.28$$

**Table 4.** SFRs, IR luminosities, and $\gamma$-ray luminosties of 1718–649 & 1146+596

| Name | $L_{8-1000\mu m}$ | $\mathrm{SFR_{IR}}$ | $\mathrm{SFR_{Ne}}$ | $\mathrm{SFR_{PAH}}$ | $L^{[\mathrm{ISM}]}_{0.1-100\,\mathrm{GeV}}$ | $L_{0.1-100\,\mathrm{GeV}}$ |
|---|---|---|---|---|---|---|
| | $\mathrm{erg\,s^{-1}}$ | $M_\odot\,\mathrm{yr^{-1}}$ | $M_\odot\,\mathrm{yr^{-1}}$ | $M_\odot\,\mathrm{yr^{-1}}$ | $\mathrm{erg\,s^{-1}}$ | $\mathrm{erg\,s^{-1}}$ |
| (1) | (2) | (3) | (4) | (5) | (6) | (7) |
| 1146+596 | $5.5 \times 10^{42}$ | $\sim 0.13$ | $0.5 \pm 0.1$ | $\sim 0.3$ | $\sim 2 \times 10^{38}$ | $\sim 0.6 \times 10^{42}$ |
| 1718–649 | $3.7 \times 10^{43}$ | $\sim 0.89$ | $1.8 \pm 0.1$ | $\sim 0.8$ | $\sim 2 \times 10^{39}$ | $\sim 2 \times 10^{42}$ |

**col(1)** — Name of the source; **col(2)** — Integrated infrared luminosity derived from archival $8-1000\,\mu$m data; **col(3)** — Star formation rate for the given integrated infrared luminosity in col(2); **col(4)** — Star formation rate calculated from Ne emission lines in Willett et al. (2010); **col(5)** — Star formation rate calculated from Polycyclic aromatic hydrocarbon (PAH) emission lines in Willett et al. (2010); **col(6)** — $0.1-100$ GeV luminosity estimated emission based on the integrated infrared flux in col(2); **col(7)** — The observed *Fermi*-LAT $0.1-100$ GeV luminosity.

# *STAR FORMATION RATE*

# *Conclusions*

- Triggering radio jets in AGN does not differentiate between elliptical hosts with substantially different fractions of young stars/star formation
- It is the jet duty cycle --- and not the jet launching itself --- which is related to the star formation rate within the host
  - Radio galaxies hosted by galaxies with more young stars are either short lived (i.e., not surviving long enough to form an extended FRII structure) or characterized by a highly modulated/recurrent jet activity.
- Comparing to the VanVelzen sample, suggests that the youngest radio sources avoid hosts with very vigorous star-formation
  - Which could be a result of an observational bias
- The gamma-ray detected 1718--649 and 1146+596, is undoubtedly related to the jet activity in the sources

# *Next Steps*

- High resolution infrared coverage of nuclear regions (JWST, Keck)
  - Spitzer data available for 14 sources
- Increasing the sample with radio measurements of CSO candidates
- Investigation of particularly interesting sources
- Expanding the scope to include Medium Symmetric Objects

# *QUESTIONS?*

# *CSO*

- CSO – Compact Symmetric Objects
- Morphological classification
- Based on the size and positioning of the radio lobes
  - Usually defined as two-sided with a projected linear size <1kpc
- This results in the jets and lobes being fully confined within their host galaxies
- Identification of CSOs requires good spatial resolution in radio observations

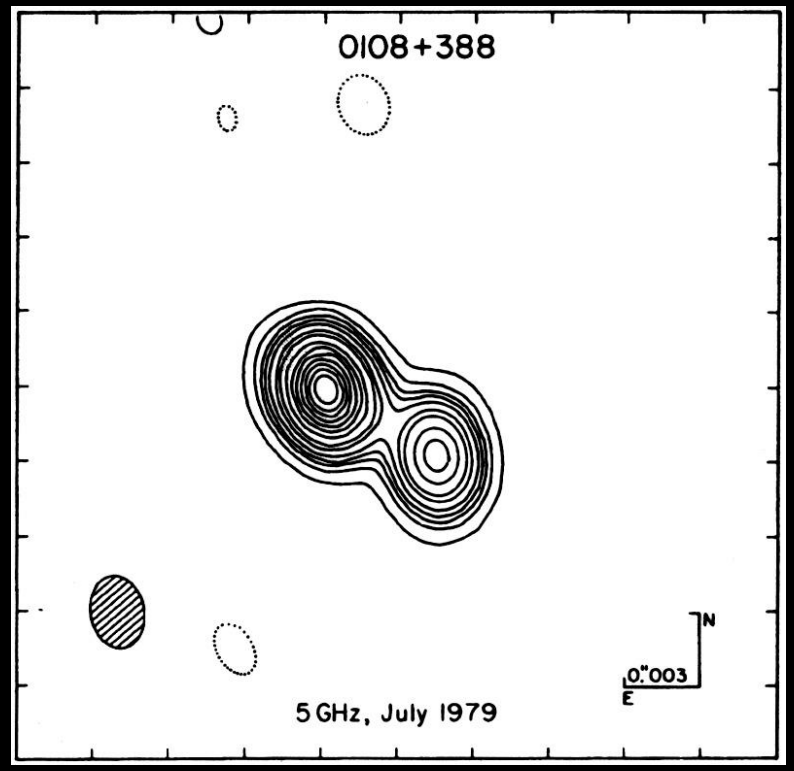


GPS/CSO source: 0108+388

Pearson, T.J, Readhead, A.C.S. 1988

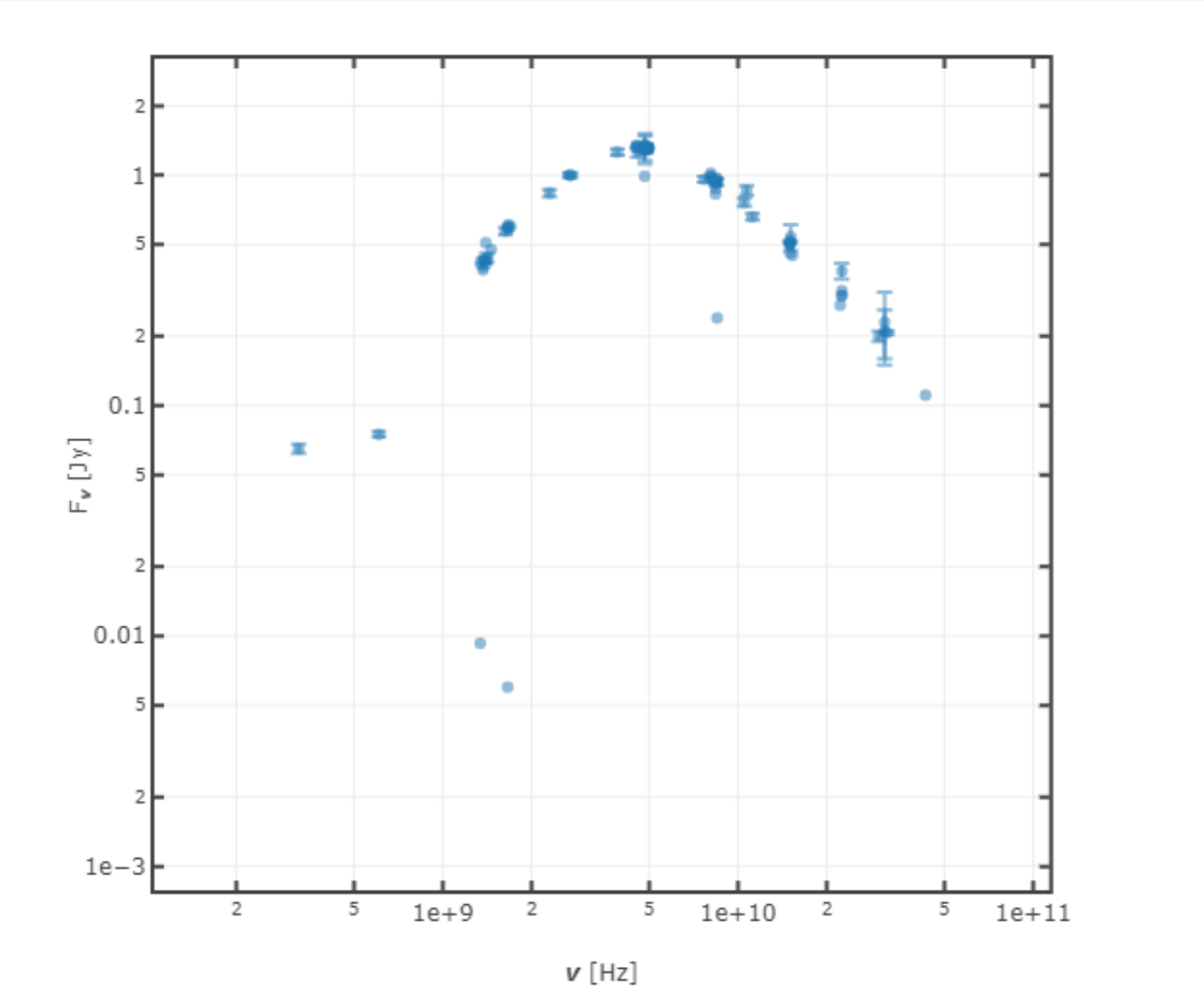


GPS/CSO source: 0108+388

# *GPS*

- GPS – GHz-peaked spectrum
- Spectroscopic classification
- The convex of the Radio spectrum around a few GHz
- The radio spectra of these small sources may appear peaked either due to synchrotron self absorption or thermal absorption
- However their spectra are steep and optically thin above the peak frequency
- The GHz-Peaked-Spectrum (GPS) sources are selected to have their radio spectra dominated by a peak in the flux density around 1 GHz (in practice in the range ~ 500 MHz to ~ 5 GHz

# *Citations*


- Asmus, D., Gandhi, P., Smette, A., H ¨onig, S. F., & Duschl, W. J. 2011, A&A, 536, A36
- Asmus, D., H ¨onig, S. F., Gandhi, P., Smette, A., & Duschl, W. J. 2014, MNRAS, 439, 1648
- Asmus, D., Gandhi, P., H ¨onig, S. F., Smette, A., & Duschl, W. J. 2015, MNRAS, 454, 766
- Giroletti, M., & Polatidis, A. 2009, Astronomische Nachrichten, 330, 193
- Migliori, G., Siemiginowska, A., Kelly, B. C., et al. 2014, ApJ, 780, 165
- O'Dea, C. P. 1998, PASP, 110, 493
- Mateos, S., Alonso-Herrero, A., Carrera, F. J., et al. 2012,MNRAS, 426, 3271
- Ostorero, L., Morganti, R., Diaferio, A., et al. 2017, ApJ, 849, 34
- Sobolewska, M., Siemiginowska, A., Guainazzi, M., et al. 2019,ApJ, 871, 71
- Stawarz,  L., Ostorero, L., Begelman, M. C., et al. 2008, ApJ, 680,911
- Siemiginowska, A., LaMassa, S., Aldcroft, T. L., Bechtold, J., &Elvis, M. 2008, ApJ, 684, 811
- Siemiginowska, A., Sobolewska, M., Migliori, G., et al. 2016, ApJ,823, 57
- Stern, D., Assef, R. J., Benford, D. J., et al. 2012, ApJ, 753, 30
- https://fermi.gsfc.nasa.gov/science/instruments/lat.html

# *Our Sample*

| Name | $z$ | $d_L$ [Mpc] | LS [pc] | class | W1–W2 [mag] | W2–W3 [mag] | *WISE* color | IRAS $L_{12\,\mu m}$ [$10^{43}$ erg/s] | MIPS $L_{24\,\mu m}$ [$10^{43}$ erg/s] | WISE $L_{12\,\mu m}$ [$10^{43}$ erg/s] | $L_{2-10\,keV}$ [$10^{43}$ erg/s] | Ref. |
|---|---|---|---|---|---|---|---|---|---|---|---|---|
| (1) | (2) | (3) | (4) | (5) | (6) | (7) | (8) | (9) | (10) | (11) | (12) | (13) |
| 0019–000 | 0.305 | 1521 | 220 | GPS | 0.472 | 2.441 | G | – | – | 3.53 ± 0.11 | 0.55^ | T09 |
| 0026+346 | 0.517 | 2852 | 190 | GPS | 0.743 | 2.491 | Un | – | – | 21 ± 0.3 | 23 ± 2 | G06 |
| 0035+227 | 0.096 | 418 | 21.8 | CSO | 0.148 | 1.265 | G | – | – | 0.425 ± 0.007 | 0.075 ± 0.034 | S16 |
| 0108+388 | 0.669 | 3907 | 22.7 | CSO | 0.132 | 3.159 | G | 9.86 ± 9.16 | 3.79 ± 1.40 | <13.1 | 7 ± 3 | T09,S16 |
| 0116+319 | 0.059 | 255 | 70.1 | CSO | 0.035 | 1.682 | S* | 0.595 ± 0.056 | 0.609 ± 0.046 | 0.629 ± 0.003 | <0.10† | S16 |
| 0402+379 | 0.055 | 234 | 7.3 | CSO | 0.099 | 1.721 | G | 0.48 ± 0.07 | 0.949 ± 0.059 | 0.608 ± 0.004 | 0.041 ± 0.016 | R14 |
| 0428+205 | 0.219 | 1044 | 653 | GPS | 0.323 | 2.648 | G | – | – | 3.93 ± 0.08 | 1.4 ± 0.6 | T09 |
| 0500+019 | 0.585 | 3319 | 55 | GPS | 1.047 | 2.892 | Q | 63.4 ± 6.5 | 87.2 ± 9.8 | 59.3 ± 0.5 | 50 ± 6 | T09 |
| 0710+439 | 0.518 | 2868 | 87.7 | CSO | 0.726 | 2.997 | Sy | 43.8 ± 4.4 | 107 ± 7 | 43.4 ± 0.4 | 39.40 ± 3.15 | T09,S16 |
| 0941–080 | 0.228 | 1100 | 148 | GPS | 0.388 | 2.444 | G* | – | – | 2.57 ± 0.05 | 0.091 ± 0.075 | T09 |
| 1031+567 | 0.460 | 2480 | 109 | CSO | 0.999 | 2.922 | Q | 17.6 ± 3.0 | 16.5 ± 4.7 | 15.6 ± 0.3 | 2.2 ± 0.2 | T09,S16 |
| 1117+146 | 0.362 | 1874 | 306 | GPS | 0.406 | 3.599 | SB | – | – | <5.87 | 1.40 ± 0.19 | T09 |
| 1146+596 | 0.011 | 47 | 933◇ | CSO• | –0.011 | 1.237 | G | 0.0816 ± 0.0022 | 0.0818 ± 0.0033 | 0.1010 ± 0.0002 | 0.007 | U05 |
| 1245+676 | 0.107 | 478 | 9.6 | CSO | 0.130 | 1.409 | G | 0.33 ± 0.14 | 0.358 ± 0.098 | 0.531 ± 0.006 | 0.031†† | W09,S16 |
| 1323+321 | 0.368 | 1908 | 247 | GPS | 0.303 | 2.014 | G | – | – | 2.54 ± 0.11 | 3.7 ± 0.4 | T09 |
| 1345+125 | 0.122 | 551 | 166 | CSO | 1.308 | 3.930 | Sy⋆ | 83.3 ± 1.7 | 216 ± 4 | 87.9 ± 0.2 | 7.8 ± 1.5 | T09,J13 |
| 1358+624 | 0.431 | 2298 | 218 | GPS | 1.210 | 2.592 | Q⋆ | 31.0 ± 2.4 | 37.8 ± 2.8 | 35.4 ± 0.2 | 30 ± 20 | T09 |
| 1404+286 | 0.077 | 336 | 10.0 | CSO | 1.018 | 3.063 | Q | 50.9 ± 0.9 | 65.2 ± 1.3 | 51.6 ± 0.1 | 0.45 ± 0.06C | T09,S16,S19b |
| 1511+0518 | 0.084 | 370 | 7.3 | CSO | 1.233 | 2.899 | Q | – | 51.1 ± 3 | 52.2 ± 0.1 | 3C | S16 |
| 1607+268 | 0.473 | 2569 | 240 | CSO | 0.287 | 2.679 | S* | 4.21 ± 3.17 | 21.6 ± 4.4 | <7.27 | 3.79 ± 0.87 | T09,S16 |
| 1718–649 | 0.014 | 60.4 | 2.0 | CSO | 0.136 | 2.462 | G | 0.322 ± 0.009 | 0.32 ± 0.01 | 0.401 ± 0.001 | 0.0154 ± 0.0024 | S16 |
| 1843+356 | 0.763 | 4612 | 22.3 | CSO | 1.160 | 4.047 | Sy | – | – | 190 ± 1 | 5.60 ± 2.28 | S16 |
| 1934–638 | 0.183 | 845 | 85.1 | CSO | 0.609 | 3.360 | Sy* | 5.89 ± 0.62 | 19 ± 1 | 6.52 ± 0.03 | 0.60 ± 0.14 | S16,S19a |
| 1943+546 | 0.263 | 1285 | 107.1 | CSO | 0.628 | 2.191 | Un | – | – | 5.64 ± 0.04 | 0.73 ± 0.28 | S16 |
| 1946+708 | 0.101 | 444 | 39.4 | CSO | 0.663 | 2.336 | Un | 1.75 ± 0.15 | 1.67 ± 0.10 | 1.69 ± 0.01 | 1.20 ± 0.18 | S16,S19a |
| 2008–068 | 0.547 | 3056 | 218 | CSO | 0.334 | 2.159 | G | – | 7.68 ± 0.35 | 9.1 ± 0.4 | 6 ± 2 | T09 |
| 2021+614 | 0.227 | 1086 | 16.1 | CSO | 1.287 | 3.009 | Q | <210 | – | 64.9 ± 0.2 | 11.2C | S16,S19a |
| 2128+048 | 0.990 | 6364 | 218 | GPS | 0.688 | 3.352 | Sy | – | 63.9 ± 2.3 | <52.4 | 29 ± 4 | T09 |
| 2352+495 | 0.238 | 1143 | 117.3 | CSO | 0.688 | 2.714 | Sy | – | – | 4.25 ± 0.04 | 1.3± 0.3 | T09,S16 |

# *MIR Luminosity*

- Infrared luminosities were derived for all 29 sources from WISE Magnitudes
- 12 micron measurements were obtained from IRAS 16 out of the 29 sources
- The 24 micron MIPS luminosities were obtained for 18 out of the 29 sources
- We note that all but four sources have comparable 24 micron MIPS luminosities to the 12 micron WISE and IRAS measurements
  - 0710+439, 1345+125, 1607+268, &1934-638
  - Show an increase of 140-210% in the 24 micron band
  - All classified as Sy, and all morphologically classified as CSOs
  - We note these four sources for further investigation in a follow-up paper, as potentially interesting sources to inspect spectroscopically.

| Name | $z$ | $d_L$ [Mpc] | LS [pc] | class | IRAS $L_{12\,\mu m}$ [$10^{43}$ erg/s] | MIPS $L_{24\,\mu m}$ [$10^{43}$ erg/s] | WISE $L_{12\,\mu m}$ [$10^{43}$ erg/s] |
|---|---|---|---|---|---|---|---|
| (1) | (2) | (3) | (4) | (5) | (9) | (10) | (11) |
| 0019–000 | 0.305 | 1521 | 220 | GPS | – | – | 3.53 ± 0.11 |
| 0026+346 | 0.517 | 2852 | 190 | GPS | – | – | 21 ± 0.3 |
| 0035+227 | 0.096 | 418 | 21.8 | CSO | – | – | 0.425 ± 0.007 |
| 0108+388 | 0.669 | 3907 | 22.7 | CSO | 9.86 ± 9.16 | 3.79 ± 1.40 | <13.1 |
| 0116+319 | 0.059 | 255 | 70.1 | CSO | 0.595 ± 0.056 | 0.609 ± 0.046 | 0.629 ± 0.003 |
| 0402+379 | 0.055 | 234 | 7.3 | CSO | 0.48 ± 0.07 | 0.949 ± 0.059 | 0.608 ± 0.004 |
| 0428+205 | 0.219 | 1044 | 653 | GPS | – | – | 3.93 ± 0.08 |
| 0500+019 | 0.585 | 3319 | 55 | GPS | 63.4 ± 6.5 | 87.2 ± 9.8 | 59.3 ± 0.5 |
| 0710+439 | 0.518 | 2868 | 87.7 | CSO | 43.8 ± 4.4 | 107 ± 7 | 43.4 ± 0.4 |
| 0941–080 | 0.228 | 1100 | 148 | GPS | – | – | 2.57 ± 0.05 |
| 1031+567 | 0.460 | 2480 | 109 | CSO | 17.6 ± 3.0 | 16.5 ± 4.7 | 15.6 ± 0.3 |
| 1117+146 | 0.362 | 1874 | 306 | GPS | – | – | <5.87 |
| 1146+596 | 0.011 | 47 | 933° | CSO• | 0.0816 ± 0.0022 | 0.0818 ± 0.0033 | 0.1010 ± 0.0002 |
| 1245+676 | 0.107 | 478 | 9.6 | CSO | 0.33 ± 0.14 | 0.358 ± 0.098 | 0.531 ± 0.006 |
| 1323+321 | 0.368 | 1908 | 247 | GPS | – | – | 2.54 ± 0.11 |
| 1345+125 | 0.122 | 551 | 166 | CSO | 83.3 ± 1.7 | 216 ± 4 | 87.9 ± 0.2 |
| 1358+624 | 0.431 | 2298 | 218 | GPS | 31.0 ± 2.4 | 37.8 ± 2.8 | 35.4 ± 0.2 |
| 1404+286 | 0.077 | 336 | 10.0 | CSO | 50.9 ± 0.9 | 65.2 ± 1.3 | 51.6 ± 0.1 |
| 1511+0518 | 0.084 | 370 | 7.3 | CSO | – | 51.1 ± 3 | 52.2 ± 0.1 |
| 1607+268 | 0.473 | 2569 | 240 | CSO | 4.21 ± 3.17 | 21.6 ± 4.4 | <7.27 |
| 1718–649 | 0.014 | 60.4 | 2.0 | CSO | 0.322 ± 0.009 | 0.32 ± 0.01 | 0.401 ± 0.001 |
| 1843+356 | 0.763 | 4612 | 22.3 | CSO | – | – | 190 ± 1 |
| 1934–638 | 0.183 | 845 | 85.1 | CSO | 5.89 ± 0.62 | 19 ± 1 | 6.52 ± 0.03 |
| 1943+546 | 0.263 | 1285 | 107.1 | CSO | – | – | 5.64 ± 0.04 |
| 1946+708 | 0.101 | 444 | 39.4 | CSO | 1.75 ± 0.15 | 1.67 ± 0.10 | 1.69 ± 0.01 |
| 2008–068 | 0.547 | 3056 | 218 | CSO | – | 7.68 ± 0.35 | 9.1 ± 0.4 |
| 2021+614 | 0.227 | 1086 | 16.1 | CSO | <210 | – | 64.9 ± 0.2 |
| 2128+048 | 0.990 | 6364 | 218 | GPS | – | 63.9 ± 2.3 | <52.4 |
| 2352+495 | 0.238 | 1143 | 117.3 | CSO | – | – | 4.25 ± 0.04 |

# Optical Images --SDSS

- 16 sources (2128+048 to faint for classification)
- Most sources are of red/yellow color
- 11 elliptical in shape
- 5 have distorted morphology
  - 0035+227
  - 0116+319 (Wise Contamination)
  - 0428+205
  - 1345+125 (Wise Contamination)
  - 1404+286 (Compton Thick)
- No distinct spiral morphology

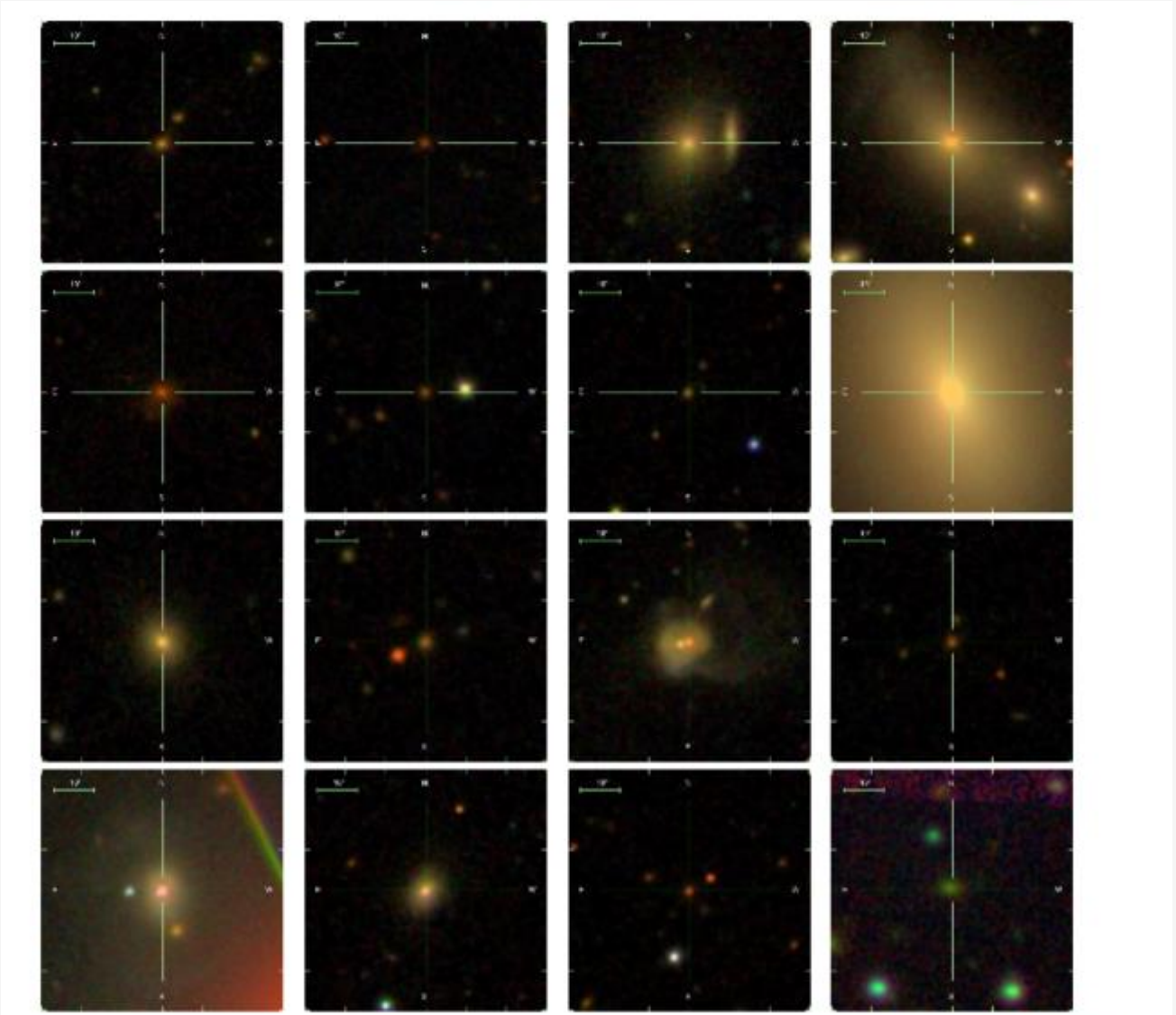

**Figure 3.** The SDSS gri color composite images of the host galaxies, available for 17 sources from our list (Aboltathi et al. 2018), excluding the particularly faint 2128+048; these are (from left to right) 0019–000, 0026+346, 0035+227, 0116+319 (first row), 0428+205, 1031+567, 1117+146, 1146+596 (second row), 1245+676, 1323+321, 1345+125, 1358+624 (third row), 1404+28, 1511+0518, 1607+268, 2352+495 (fourth row). In each image, the position of the source is indicated by a cross, while the image scale is shown in the upper left corner, with each image being a square 60″.

# Optical Images --PanSTARRS

For the remaining sources which are not covered by the SDSS, or which are too faint for the SDSS, we retrieved the optical images of the hosts from the all sky survey PanSTARRS in the i band (7563 angstroms)

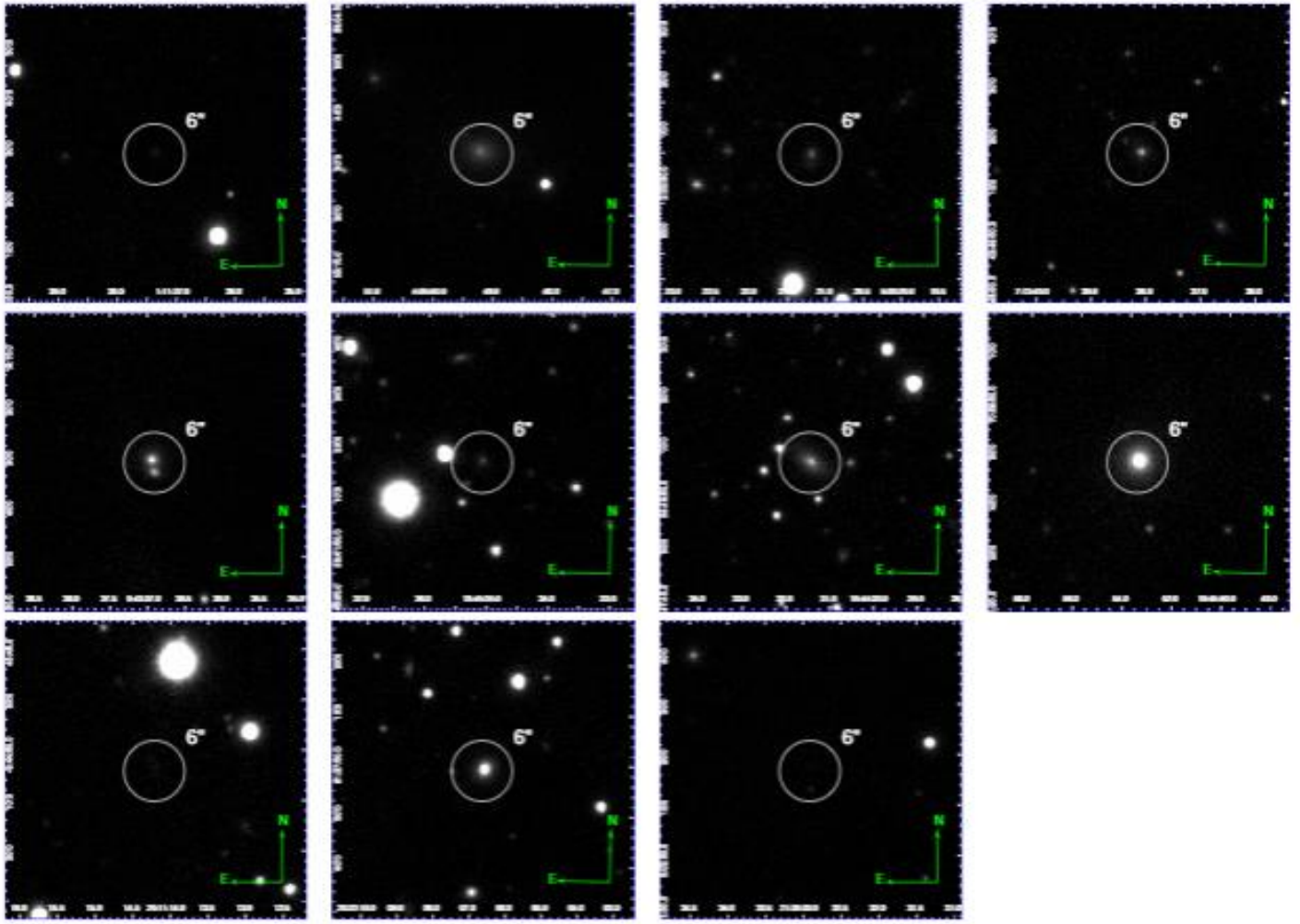


**Figure 4.** Optical images of sources not covered by SDSS (or too faint for SDSS), but observed instead by the all sky survey PanSTARRS, in the i band (7563 Å), including (from left to right) 0108+388, 0402+379, 0500+019, 0710+439 (first row), 0941–080, 1843+356, 1943+546, 1946+708 (second row), 2008–068, 2021+614, and 2128+048 (third row). In each image with overlaid ecliptic coordinate grids, the position of the source is indicated by a circle with a diameter of 6″ with each image being a square 60″.

# Optical Images -- Super Cosmos Sky Survey

In the case of the two southernmost objects 1718-649 and 1934-638, from the Super Cosmos Sky Surveys in the UKST blue band

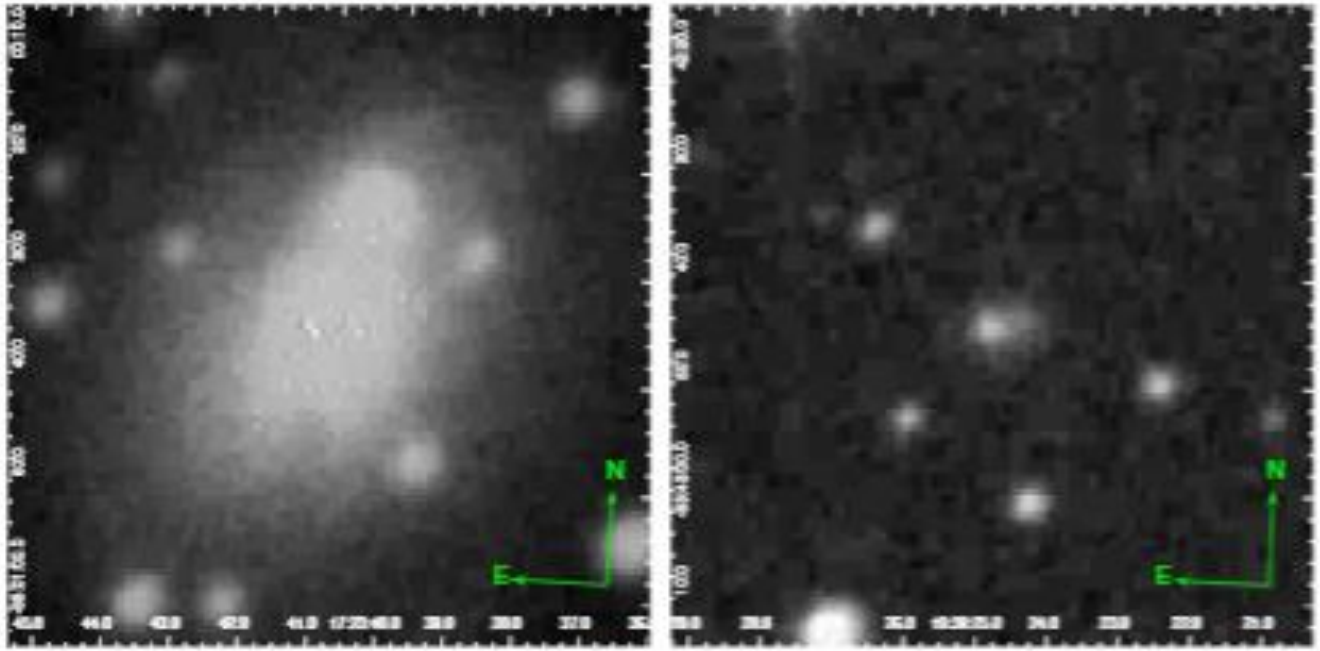


**Figure 5.** Additional optical images in the UKST blue band of the two southernmost sources 1718–649 (left panel) and 1934–638 (right panel), obtained from the Super Cosmos Sky Surveys. In each image, the position of the source is in the center of the image with each image being a square 60″ and containing overlaid ecliptic coordinate grids.

# *Optical Images*

- These images are shown as strictly optical intensity and as such  no comments on their colors are made.
- We note that 0108+388, 2008--068, and 2128+048 are too faint in optical for any classification.
- Again, most of those galaxies whenever bright enough to be classified morphologically, display elliptical shapes, with the exception of the peculiar 1718--649 host, ``having the appearance of a high luminosity elliptical with faint outer spiral structure" as noted by Fanti et al. (2000)

# *Xray vs Xray/IR*

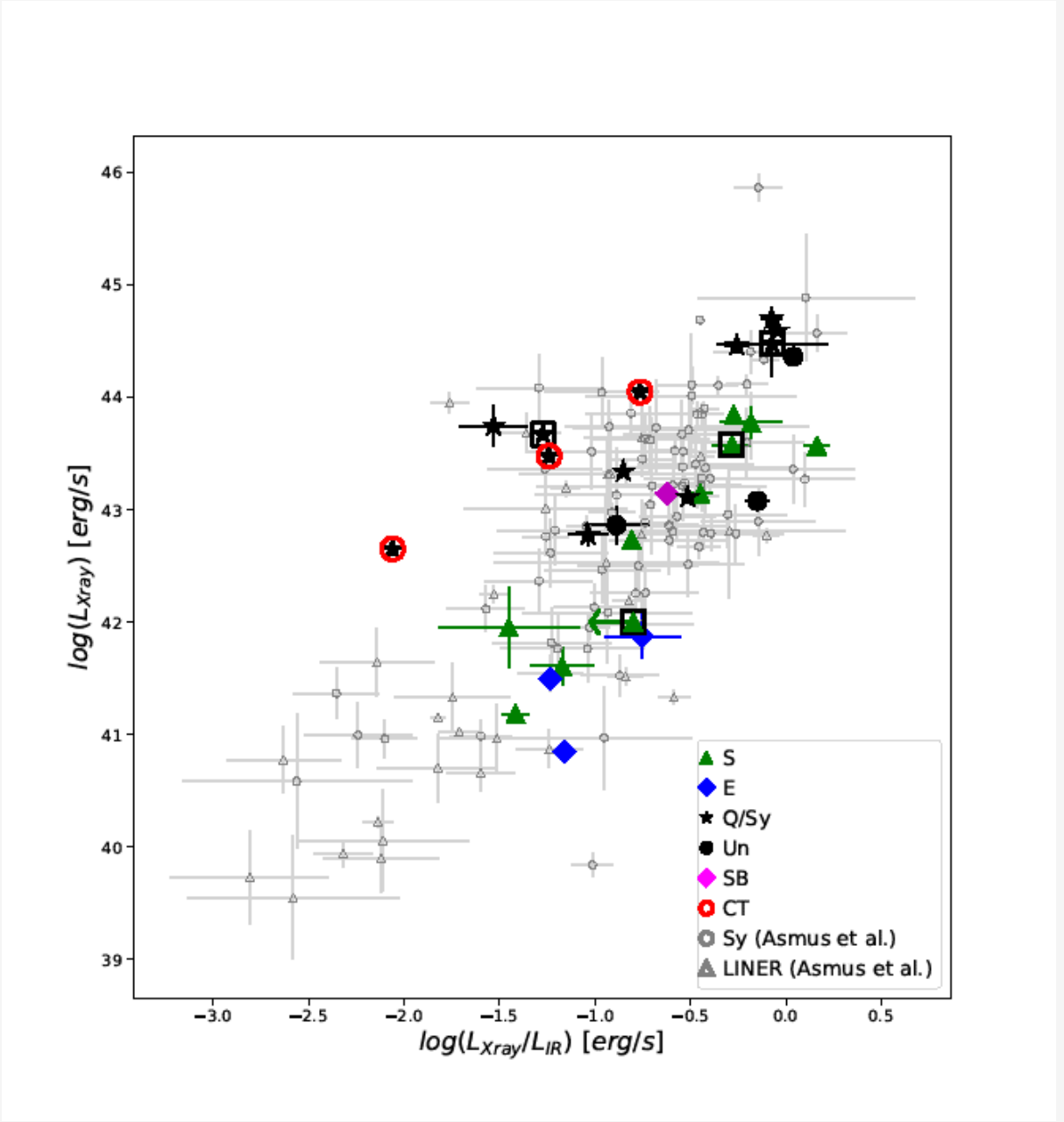

# *IR vs XRAY/IR*

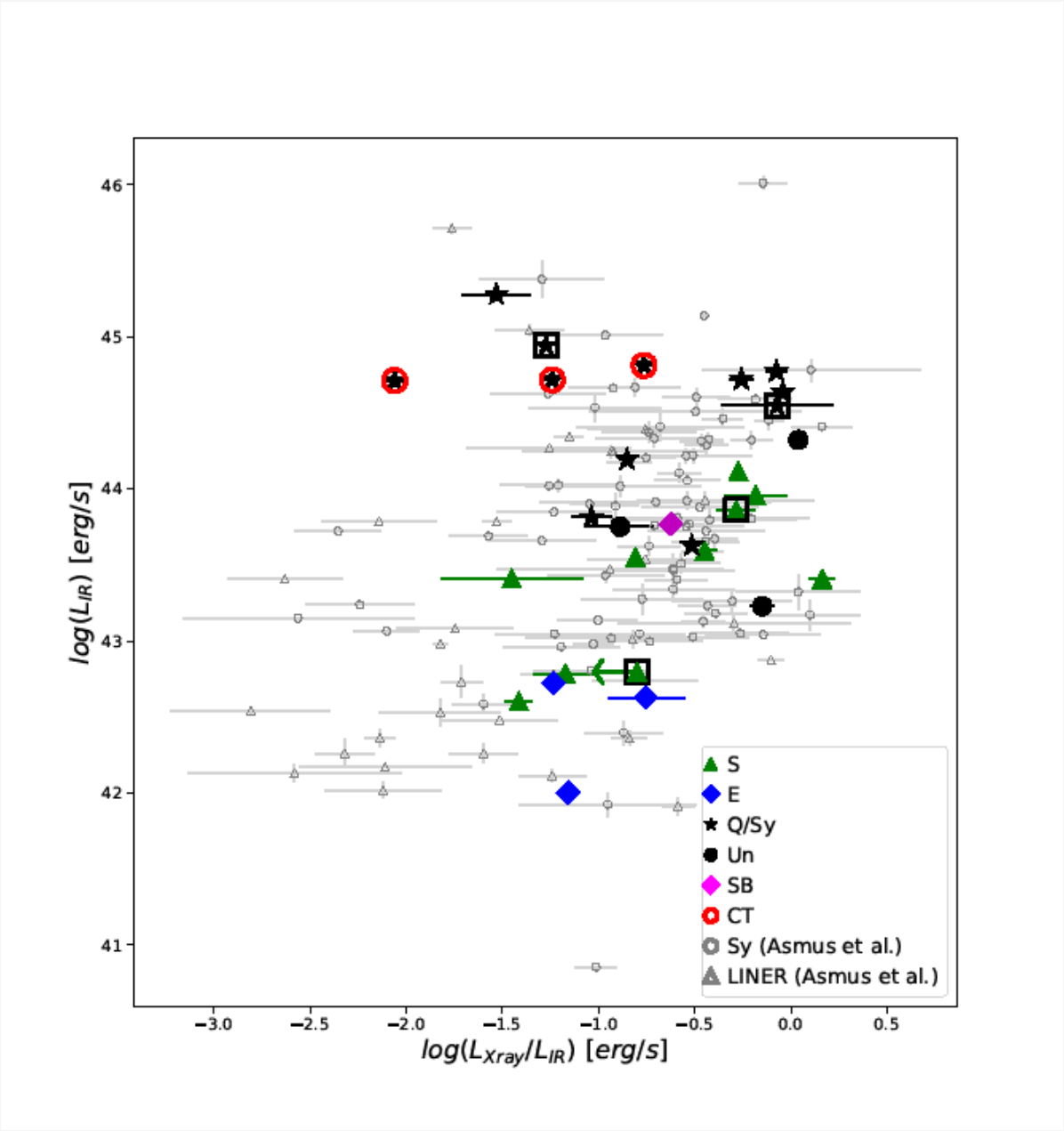
46
45
44
43
42
41
log(L_IR) [erg/s]
−3.0
−2.5
−2.0
−1.5
−1.0
−0.5
0.0
0.5
log(L_Xray/L_IR) [erg/s]
S
E
Q/Sy
Un
SB
CT
Sy (Asmus et al.)
LINER (Asmus et al.)

# MIR/XRAY Correlation Z-cut

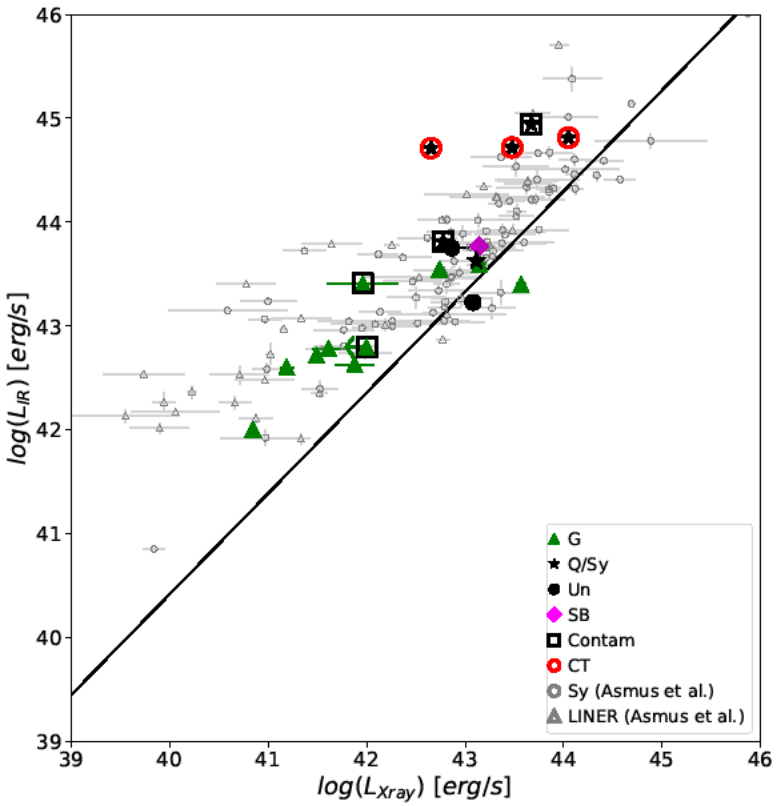


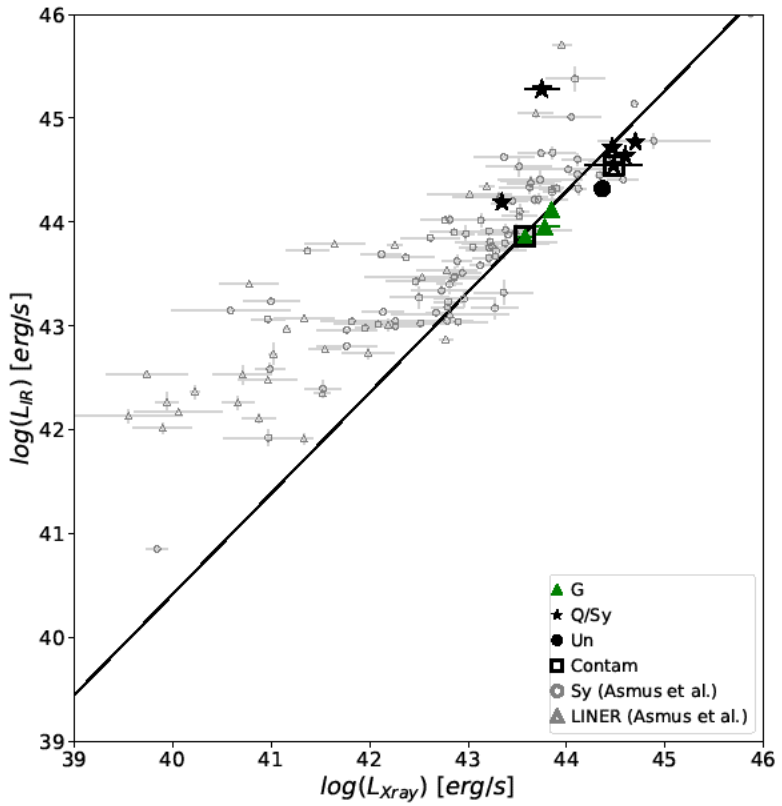


**Table 3.** IR–Xray 2D KS Test Results

| Sample Set | $p$-value | $D$ value |
|---|---|---|
| Full Sample | 0.10 | 0.26 |
| $z < 0.4$ | 0.25 | 0.26 |
| $z > 0.4$ | $1.8 \times 10^{-4}$ | 0.7 |

- Asmus et al. 2015 sample (small grey symbols) with our 29 CSO/GPS sources (large symbol)
- Left: Sample of our sources z<0.4
- Right: Sample of our sources with z>0.4